FOI-R--1246--SE
June 2004
ISSN 1650-1942
Technical report

Mats Bäckström, Olof Lundén

Experimental Investigation of Degradation and Non-Linear Effects in Corroded EMC Joints Exposed to High Power Microwaves (HPM)

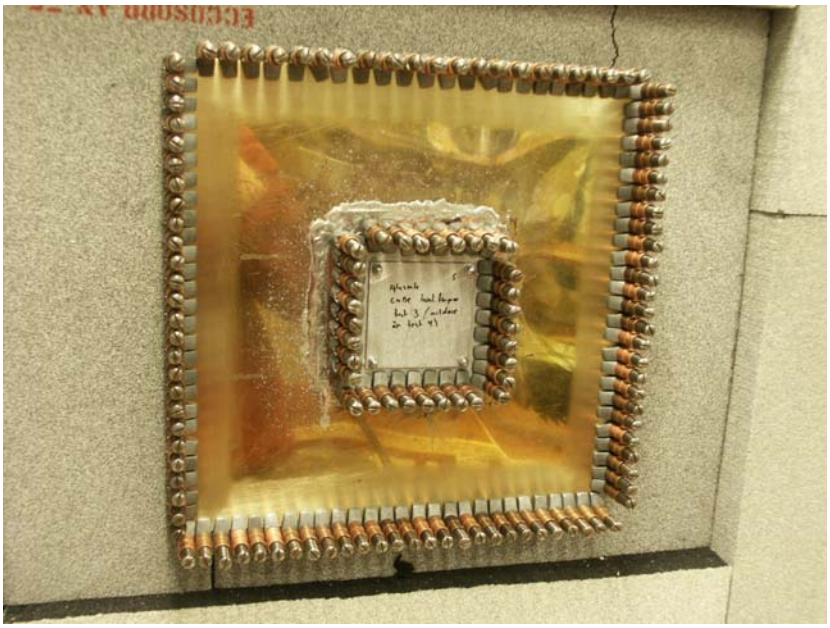

Sensor Technology
SE-581 11 Linköping

SWEDISH DEFENCE RESEARCH AGENCY

Sensor Technology
P.O. Box 1165
SE-581 11 Linköping

FOI-R--1246--SE

June 2004

ISSN 1650-1942

Technical report

Mats Bäckström, Olof Lundén

Experimental Investigation of Degradation and Non-Linear Effects in Corroded EMC Joints Exposed to High Power Microwaves (HPM)

Issuing organization	Report number, ISRN	Report type
FOI – Swedish Defence Research Agency Sensor Technology P.O. Box 1165 SE-581 11 Linköping	FOI-R--1246--SE	Technical report
	Research area code 6. Electronic Warfare and deceptive measures	
	Month year June 2004	**Project no.** E3031
	Customers code 5. Commissioned Research	
	Sub area code 61 Electronic Warfare including Electromagnetic Weapons and Protection	

Author/s (editor/s)	Project manager
Mats Bäckström Olof Lundén	Mats Bäckström
	Approved by
	Sponsoring agency Swedish Armed Forces
	Scientifically and technically responsible

Report title

Experimental Investigation of Degradation and Non-Linear Effects in Corroded EMC Joints Exposed to High Power Microwaves (HPM)

Abstract (not more than 200 words)

Determination of shielding effectiveness is a vital part in the analysis of a systems capability to withstand HPM. It is usually assumed that the shielding effectiveness, determined at low field levels, is valid at HPM threat levels. This assumption might be refuted by the presence of non-linear effects, e.g. due to electrical discharge or metal-insulator-metal junctions caused by corrosion (the "rusty bolt effect"). Non-linear effects may result in damage of the shielding joint and/or in generation of new frequency components in the spectrum of the transmitted pulse. Measurements have been performed on 31 corroded EMC joints. No major degradation could be detected after HPM irradiation at 3 GHz. Also, most of the objects showed only limited changes of the time domain shape of the transmitted pulse. Most of the objects showed none, or only a moderate generation, of harmonics. However, many of these latter objects indicate a significant spectral content below and around 1 MHz. A preliminary analysis, made difficult by present measurement set-up, indicates that the energy content of the transmitted pulse at low frequencies in some cases might be of the same order as that around 3 GHz. This will be further investigated in the future.

Keywords

HPM, shielding, corrosion, non-linear, degradation, EMC

Further bibliographic information	**Language** English
ISSN 1650-1942	**Pages** 49 p.
	Price acc. to pricelist

Utgivare	Rapportnummer, ISRN	Klassificering
Totalförsvarets Forskningsinstitut - FOI	FOI-R--1246--SE	Teknisk rapport
Sensorteknik	**Forskningsområde**	
Box 1165	6. Telekrig och vilseledning	
581 11 Linköping	**Månad, år**	**Projektnummer**
	Juni 2004	E3031
	Verksamhetsgren	
	5. Uppdragsfinansierad verksamhet	
	Delområde	
	61 Telekrigföring med EM-vapen och skydd	

Författare/redaktör	Projektledare
Mats Bäckström	Mats Bäckström
Olof Lundén	**Godkänd av**
	Uppdragsgivare/kundbeteckning
	Försvarsmakten
	Tekniskt och/eller vetenskapligt ansvarig

Rapportens titel (i översättning)

Experimentell undersökning av degradering och olinjära effekter i korroderade skärmfogar som utsatts för Högeffekt Pulsad Mikrovågsstrålning (HPM)

Sammanfattning (högst 200 ord)

Bestämning av skärmverkan utgör en viktig del i utvärderingen av ett systems tålighet mot HPM. Vanligtvis antas att den skärmverkan som uppmätts vid låga fältnivåer är giltig också vid extrema hotnivåer. Detta antagande kan tänkas vara felaktigt p.g.a. uppkomsten av olinjära effekter, t.ex. beroende på elektriska urladdningar eller på förekomsten av metall-isolator-metall övergångar orsakade av korrosion. Olinjära effekter kan orska skador på skärmfogen och/eller att nya frekvenser uppstår i den transmitterade pulsens spektrum.

Mätningar har utförts på 31 korroderade skärmfogar. Ingen uppenbar degradering kunde fastställas efter att skärmfogarna utsatts för HPM vid 3 GHz. De flesta provobjekten uppvisade också bara små förändringar i utseendet (tidsdomän) av den transmitterade pulsen. De flesta objekten uppvisade ingen, eller bara en måttlig genering av övertoner. Emellertid tycks flera av dessa senare objekt uppvisa ett påtagligt frekvensinnehåll under och vid 1 MHz. En preliminär analys indikerar att energiinnehållet i den transmitterade pulsen i vissa fall kan vara av samma storleksordning vid låga frekvenser som vid 3 GHz. Analysen försvåras emellertid av den nuvarande experimentuppställningens låga känslighet vid låga frekvenser, varför detta fenomen skall undersökas vidare.

Nyckelord

HPM, skärmning, korrosion, olinjär, degradering, EMC

Övriga bibliografiska uppgifter	**Språk** Engelska
ISSN 1650-1942	**Antal sidor:** 49 s.
Distribution enligt missiv	**Pris: Enligt prislista**

Table of Contents

1 Background

In later years a growing attention has been paid to the threat posed by HPM (High Power Microwaves) against the function of important electronic systems, military as well as civilian. A vital part in the analysis of a complex systems capability to, without serious malfunction, withstand HPM irradiation is to determine the shielding effectiveness of various parts of its structure. In e.g. the case of an aircraft it is important that the avionics bays provide a sufficiently well shielded environment, in order to reduce the external HPM threat to levels that can be tolerated by the avionic equipment located within the bay. The analysis of the shielding properties of an equipment bay or an electronic enclosure is usually made by a combination of measurements and theoretical modelling, in the latter case often by use of numerical analyses. In both these cases it is usually assumed that the transfer function from the external to the internal environment is linear, i.e. it is assumed that the results determined at low field levels are also relevant at high field levels, i.e. at the actual HPM threat levels. This report addresses the question whether this assumption is valid. The assumption could be refuted by the presence of non-linear effects such as electrical discharges in thin slots or the existence of metal-insulator-metal junctions caused by corrosion (the “rusty bolt effect”).

Non-linear effects may result in generation of harmonics. Electrical discharges may also result in a reduction of the total transmitted electromagnetic power through the aperture. Thus, the appearance of electrical discharges would probably be beneficial since it would reduce the amount of energy leaking into the shielded compartment. However, negative effects could counterbalance this beneficial reduction in transmitted energy. One reason could be the generation of harmonics, including low frequency components, another could be damage of the gasket or of the surface treatment (such as chromated coatings) in the seam. This report deals mainly with the generation of harmonics and the detection of damage or degradation of the shielding effectiveness of the seam. The third effect, the reduction of transmitted energy, has also been studied by us (primarily as a possible method to protect array antennas) and reported separately. Some of these results will, however, also be presented here.

If generation of harmonics should turn up to be of importance the expected low frequency content, caused by envelope detection (resulting from the non-linear processes) of the pulsed microwave signal, would probably be of most interest. The reason being that electronic equipment is usually more susceptible to frequencies below microwave frequencies.

Measurements have been performed on EMC joints subjected to corrosion as well as on thin slots and a generic riveted seam. The corroded EMC joints have kindly been put to our disposal by SCI, the Swedish Corrosion Institute, and co-operating industries, see [8, 9].

The research has been carried out within the FOI *HPM protection project* financed by the Swedish Armed Forces. This report covers the work done until May 2004.

2 Measurement Set-ups

2.1 High-level tests.

2.1.1 General.

The measurement set-up for high field level assessment is located inside a shielded room. It consists of a 700 kW, 3 GHz, S-band magnetron. In the present investigation, the pulse length was 1 μs and the pulse repetition frequency around 70 Hz. The field is radiated by means of a waveguide horn antenna having a gain of 15 dB_i. The 3 dB lobe width is approximately 30 degrees. The AUT (Aperture Under Test) is mounted on a 30x30 cm flange mounted on an approximately one cubic meter large aluminium box; see Figure 1. A block diagram of the system is shown in Figure 2. The output signal from the magnetron is extracted using a directional coupler and a power splitter and connected to a Tektronix TDS-6604 oscilloscope. via a semi-rigid cable. The oscilloscope has an analogue 3 dB bandwidth of 6 GHz and a maximum sampling frequency of 20 GHz. The number of data points can be up to 200 000 which for a sampling interval of 50 ps yields a total sampling time of 10 μs. A picture of the oscilloscope is given in Figure 3. The control room houses, apart from the oscilloscope, also a pulse generator which triggers the magnetron and the control for the wave-guide switch that decide if the output power from the magnetron shall be transmitted through the horn antenna or dumped in a dummy load. The electric field strength at the AUT is varied by moving the aluminium box along a rail. This result in electric field strength variations from typically 5.6 kV/m, at the distance of 3000 mm up to 100 kV/m at a distance of 0 mm, see Figure 4. The distance refers to the distance from the physical aperture plane of the horn antenna. The calibration of the electric field strength is described in paragraph 2.1.2 below.

At the higher fields strengths the AUT will be irradiated at near-field conditions. Commonly, the far-field boundary for antennas, R, is derived (or defined) using the following expression [2, p.24]:

$$R = \frac{2 \cdot D^2}{\lambda} \qquad (1)$$

where D is the maximum dimension of the antenna, or of the test object if that is larger, and λ is the wavelength. The horn antenna has $D = 240$ mm, which gives $R = 1152$ mm, i.e. the far field limit is at approximately 1.2 meter. This corresponds to a field strength of approximately 15 kV/m. This is roughly consistent with measured data which show evident near-field effects for field strengths at and above around 20 kV/m (distances shorter than around 700 mm), see next paragraph.

The signal transmitted through the AUT is detected by a D-dot sensor (Prodyn type AD-20 [16]) located inside the aluminium box, close behind the AUT, about 4 cm behind the plane of the flange, see Figure 5. The probe has been fixed in the same position during all measurements.

In order to avoid reflection inside the aluminium box it is loaded with absorbing material, ferrite tiles on the floor and absorbers on (most of) the walls. The reason is that we want to decrease the quality factor to avoid frequency broadening due to ringing of the box, cf. the discussion in paragraph 4.2 .The D-dot probe is connected to a balun (Prodyn type BIB-100 G [16]), see Figure 6. The signal is, via a step-attenuator and a semi-rigid cable connected to the oscilloscope. The attenuator and the cable losses are calibrated at 3 GHz. In performing the

measurements it became obvious, at least for test objects showing a high attenuation (i.e. good shielding), that a semi-rigid cable had to be used in order to provide good isolation of the external field to the oscilloscope.

A user's manual of the system is given in [1].

Figure 1. Measurement set-up. 700 kW, 3 GHz, magnetron to the right, transmitting horn antenna to the left. The aperture under test is mounted on a flange on the aluminum box "the kiosk". In the picture the box is located on the rail at a distance of 4284 mm.

.

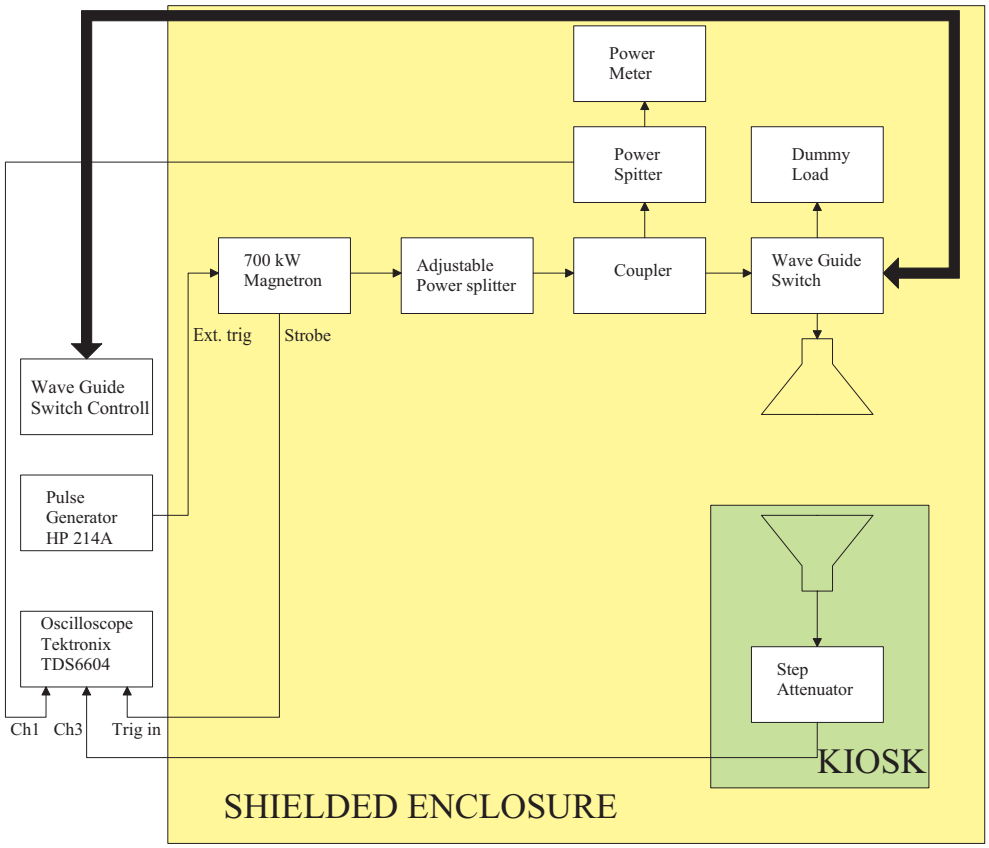

Figure 2. The measurement system. Block diagram

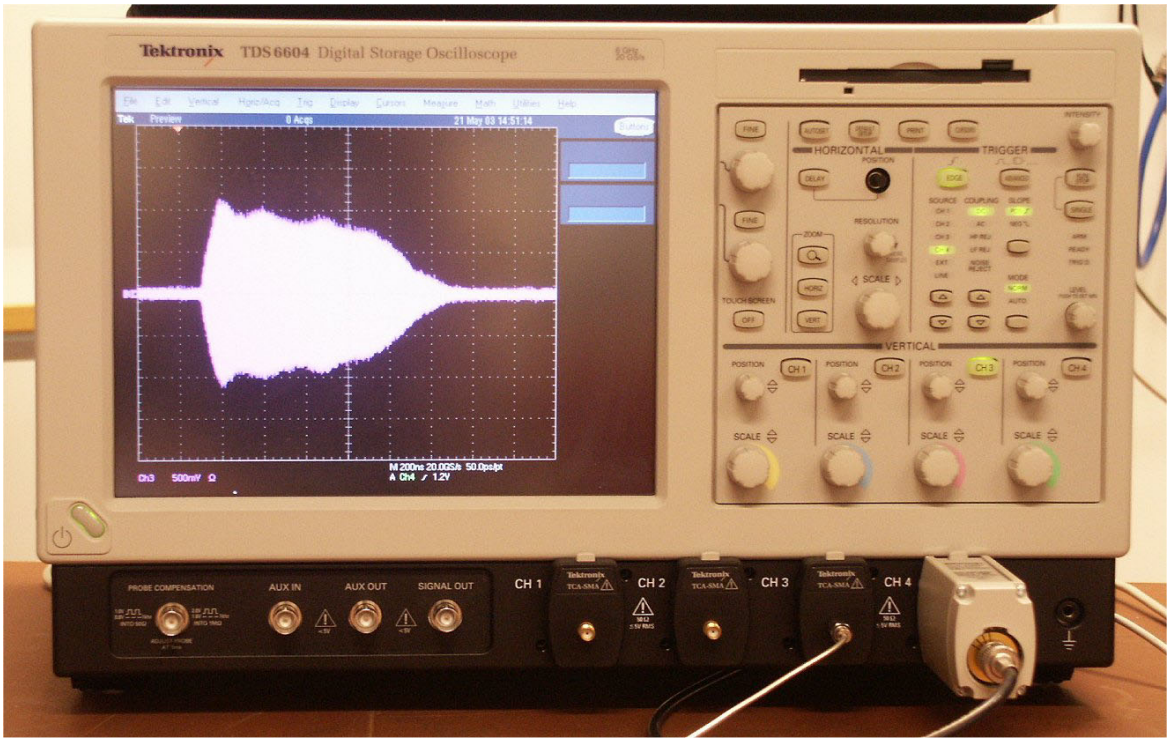

Figure 3. The 3 GHz, 1µs, output signal from the magnetron. 200 ns/div 20 GS/s 50 ps/pt 500 mV/div

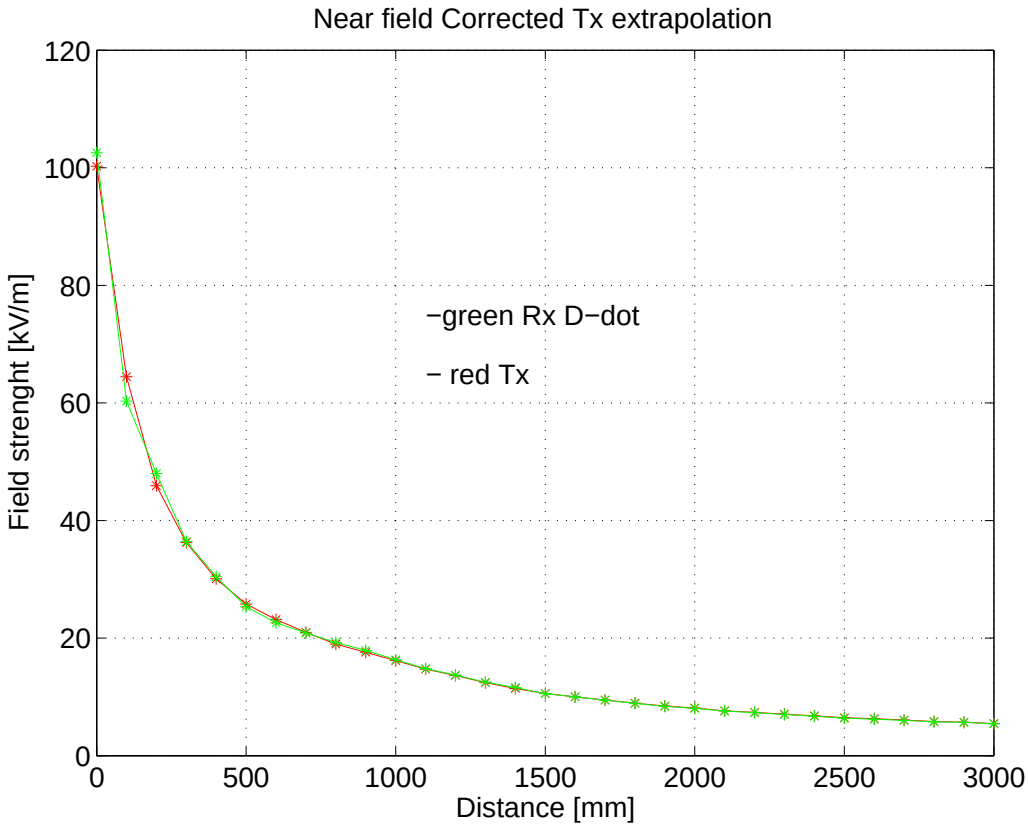

Figure 4. Typical field strength as function of the distance along the rail. Green curve measured using D-dot probe. Red curve derived from magnetron output signal.

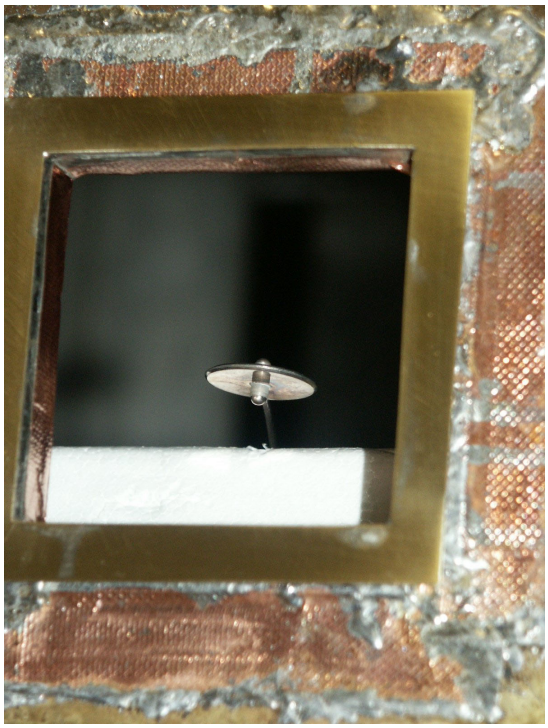

Figure 5. D-dot sensor mounted behind the AUT.

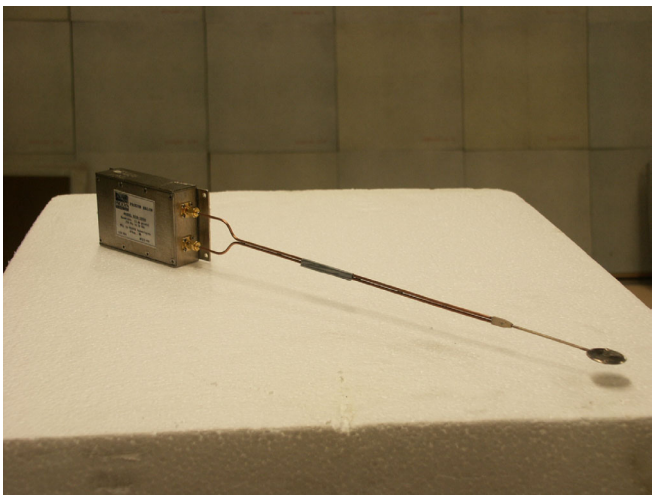

Figure 6. D-dot sensor connected to the balun.

2.1.2 Calibration of the incident field

The electric field strength incident on the aperture under test, was measured using the D-dot sensor and the balun, see Figure 5 and 6. The output power from the magnetron was kept constant. The typical setting of the magnetron is described in [1]. The sensor was placed on a Styrofoam block; see Figure 7 and 8. The total measured field consists of the direct wave from the horn antenna and to a certain extent also from reflections on the walls of the shielded room. The room is lined with absorbers only at the back wall; see Figure 1. This means that the field irradiating the AUT is slightly different from the field irradiating the omni-directional D-dot sensor. The measured field is given in Figure 4, green curve. In the figure we also show the field derived from the measured output power from the magnetron. The calculation is essentially based on a polynomial fit [1].

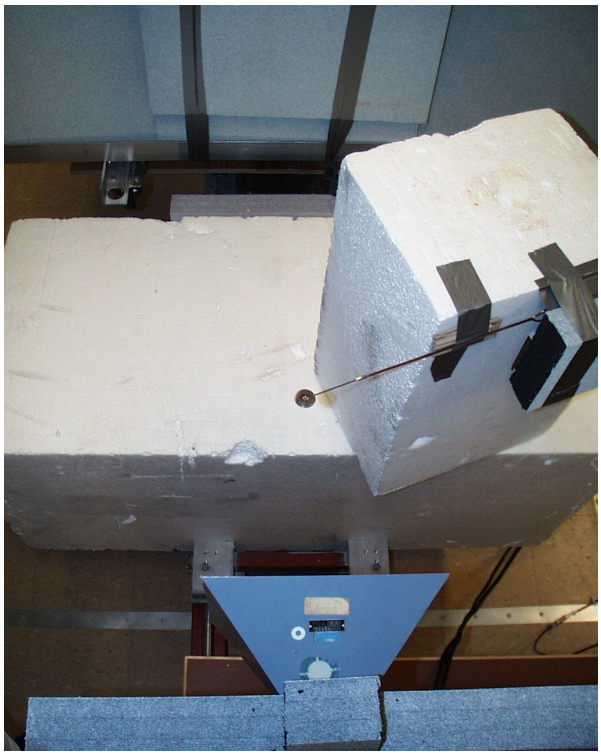

Figure 7. Calibration set-up viewed from above. D-dot sensor and transmitting antenna.

Figure 8. D-dot sensor and transmitting antenna viewed from the aperture under test.

The field was, apart from using the D-dot probe, also calibrated using the same kind of standard gain horn antenna as the transmitting one (Waveline type 299). In this case the electric field strength was calculated assuming a wave impedance of 377 Ohm, i.e. far field conditions. The resulting calibration curve is, together with the D-dot measurement, shown in Figure 9. As can be seen in the figure the curves show a systematic deviation below a distance of about 700 mm, corresponding to an electric field strength of about 20 kV/m. We ascribe this deviation to the near field conditions at these distances, cf. the discussion on paragraph 2.2.1 above.

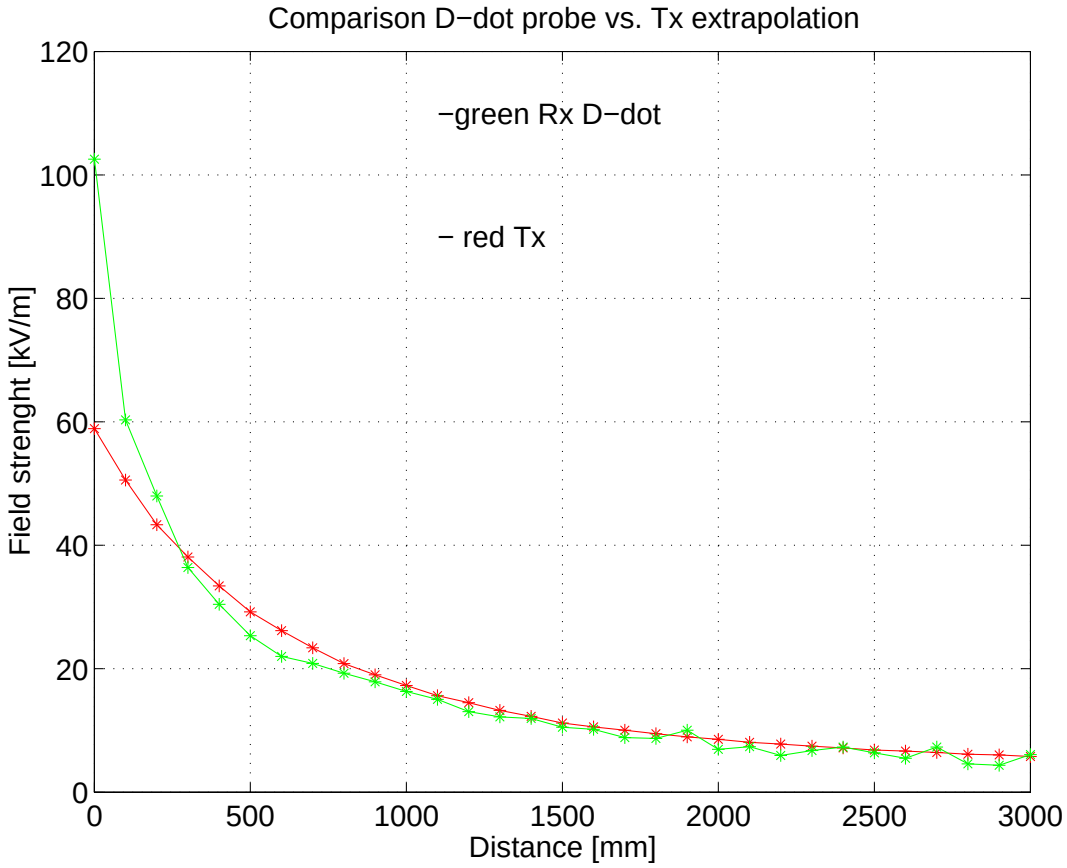

Figure 9. Comparison between the electric field strength measured by the D-dot probe (green curve) and the field strength calculated from a measurement using the receiving horn antenna (red curve). The latter calculation was made assuming a wave impedance of 377 Ω.

2.2 Aperture transmission cross-section. Low-level measurements.

The shielding properties of the apertures-under-test (AUT) were determined by measuring the transmission cross-section, using FOI's reverberation chambers. In order to evaluate possible damage or degradation of the shielding joints the cross-sections were measured both before and after exposure to the high field levels. The usefulness and benefits of the concept of transmission cross-section compared to traditional ways of characterizing the shielding properties of apertures, together with a description of the measurement procedure, can be found in [3-7]. In the present case the absolute values of the transmission cross section of the test objects were achieved by normalizing the measured data for the test objects to the corresponding data for a 30 mm diameter circular hole. The transmission cross section for such an aperture has been determined earlier by a calibration procedure of the chambers and validated by comparisons to analytical expressions of the cross section [3,4].

The transmission cross section, σ_a, is defined (under CW conditions) as the power transmitted through the aperture normalized to the power density of the incident field, S_{inc}:

$$P_t = \sigma_a \cdot S_{inc} \qquad (2)$$

where P_t is the power transmitted through the aperture. From Equation (2) it follows that the dimension of σ_a is given in square meters. In general (for plane wave conditions) the transmission cross section will depend on the polarization and angle of incidence of the plane wave exciting the aperture. In a reverberation chamber, the measured σ_a corresponds to an isotropic average of plane waves arriving from all (or rather many) possible angles of incidence and polarizations from the half space irradiating the aperture. In the present case the measurement is carried out using two reverberation chambers connected by a common opening containing the AUT. The incident field is generated in one of the chambers and the transmitted power is measured, using a calibration procedure, in the other.

Interiors from the reverberation chambers are shown in Figure 10 and Figure 11. More details about the measurements can be found in [8].

Figure 10. Measurement of aperture transmission cross-section in FOI reverberation chambers. Stirrer in the ceiling, receiving antenna in the front, fixture with test object mounted on a common panel between the two chambers.

Figure 11. Aperture under test mounted in the reverberation chamber. A brass fixture covers a 290x290 mm opening between two chambers. The test object is mounted, using wave-guide clamps, over an 80x80 mm hole in the common panel brass fixture.

2.3 Measurement uncertainty

2.3.1 High level testing

In the high power investigation the uncertainty is considered to depend mainly on undesired reflections around the test set-up. It also depends on the signal level, which determines how many of the 8 bits in the A/D converter that are in use, and on the uncertainty of the instruments. A typical uncertainty of the measured value of the incident field is estimated to less than ± 1 dB. This is calculated from the far field data shown in Figure 3 in [13]. The uncertainty is probably smaller at distance below 1500 mm, presumably better than ± 0.5 dB,

as can be concluded from Figure 3 in [13]. We here assume that the deviations at far field distances, i.e. above around 1.2 meter are due to reflections in the room (i.e. they are authentic), while the large deviation shown in that figure at very short distances, 200 mm and below, are assumed to result from near field effects. In the near field the D-dot probe, being a calibrated electric field sensor, is of course far more reliable for measuring the electric field strength than the horn antenna. In the high level experiments all the measurements of the field transmitted through the AUTs (except for the thin slot) are given in absolute values. (For the thin slot the transmitted field was measured using a horn antenna of the same sort as the antenna used for the irradiation [1,13].) However, the absolute values of the fields transmitted through the AUTs are not of primary interest in our investigation. The reason is that we look for possible generation of new frequency components due to non-linear effects, and the relative magnitude of these components with respect to the spectrum when no such effects occur. Note that the absolute values of the electric field strength shown in the time domain plots are based on the D-dot calibration factor at 3 GHz. This means that if large harmonics are created this calibration factor is no longer exactly valid. This could possibly be the case for the non-typical result shown in Figure 27a (test object L38). As will be discussed later further investigations will be made to evaluate this interesting case.

In the measurements of the corroded seams 80 000 samples were collected with 50 picoseconds sample interval. The test channel (the pulse transmitted through the aperture under test) and the reference channel (the output pulse from the magnetron measured in oscilloscope Ch1, see Figure 2) were measured simultaneously. Ten pulses were acquired for each measurement, i.e. for each given test panel at each distance.

In the measurements we were looking, as an indication for the presence of non-linear effects, for harmonics at 6 and 9 GHz, see Chapter 4. From the reference signal measured in the wave-guide a 6 GHz component, generated by the magnetron itself, could be seen. When measured with the 29x29 cm hatch open, see paragraph 4.4, we see that this component is, on the average, about 51 dB below the peak level at 3 GHz.

In order to compare the electric field strength behind the AUT at different frequencies a Fast Fourier Transform (FFT) using MATLAB (The Math Works, Inc.) was applied on the time domain data from the D-dot probe. The resulting frequency domain data have to be divided by the frequency, since the D-dot probe is a derivative type of sensor. In the derivation of the frequency plots we have assumed that loss in the Balun as well as the loss in the attenuator between the Balun and the oscilloscope is frequency independent, cf. [13]. The uncertainty due to this assumption is estimated to be typically less than ± 0.5 dB. The 3 dB bandwidth of the Balun is claimed to be 250 kHz to 10 GHz [16].

Since the D-dot probe is derivative the signal level at low frequencies becomes very low. As will be shown later, discussing the results of the measurements, this makes it very difficult to reveal a possible low frequency content of the signal.

2.3.2 Transmission cross section

The uncertainty of a measurement of the transmission cross section in a reverberation chamber is essentially due to the statistical nature of the reverberation chamber technique, i.e. not by the uncertainty of the instruments used. In the present case we have selected to use 10 x 10 stirrer positions. The uncertainty can be estimated by use of Eq. (27) in [3]. This gives an uncertainty of about ± 1.6 dB.

3 Test Objects

The test objects consist mainly of EMC joints that have been subjected to corrosion. These objects represent selections taken from two studies headed by the Swedish Corrosion Institute (SCI) in Stockholm.

The first study was initiated in 1994 and issued its final report in 1999 [9]. The study was carried out in co-operation with 10 Swedish industries and one Finnish industry. The influence of accelerated corrosion on the shielding properties of different material combinations used in joints was studied using near-field measurements between 20 MHz and 2 GHz. From the summary of [9] we quote: "The accelerated corrosion tests involved the exposure to cyclic variations in temperature and humidity and addition of SO_2, NO_2 and Chloride. The results of the near field measurement of aluminum, galvanized steel, aluzink, stainless steel and magnesium in combination with different gaskets and contact fingers shows that large decrease in shielding effectiveness was observed for joints with CuBe and tin plated contact fingers. For joints with gaskets of carbon filled PTFE an increase and for silver filled elastomer a smaller decrease in shielding effectiveness was observed after the corrosion tests. A decrease in shielding effectiveness was also obtained for joints of galvanized steel, aluzink and stainless steel without conductive gaskets or contact fingers."

The second study started in 2000 and issued its final report in 2004 [8]. The study was carried out in co-operation with 5 Swedish industries and one Finnish industry. The influence of corrosion from a one-year weather protected outdoor exposure on the shielding properties of different material combinations was studied. Both near-field measurements at SCI, between 100 MHz and 2 GHz, and absolute measurements of the transmission cross section, between 2 and 18 GHz, in FOI's reverberation chambers, were made. From the summary of [8] we quote: "Effects of corrosion have been found to differ between different gasket types, also with the same material combination….Chromate conversion coatings, on aluminum as well as on an aluminum-zinc hot-dip coating, have been found to slightly impair shielding performance….Some effects of galvanic corrosion have been found, e.g. from contact between aluminum and a copper alloy. The often good contact properties (low D.C. resistance) of tin plated contacts have been found to be reflected by the good performance joints with tin-tin contacts."

Beside of the objects from the SCI studies we have also investigated simple slots and a riveted seam. Results from one of the slot geometries are included here since they illustrate the effects at electrical breakdown, such as spectral broadening and reduction of transmitted power and energy.

3.1 Thin Slots and riveted seam

Several slots have been investigated; see [11, 12]. These include slots with needle in the middle of the gap, with the aim to create a local field enhancement at the tip of the needle. Also investigations have been made regarding the influence of placing a radioactive preparation (Americium, Am-241) close to the slot. Since the results from these studies have been presented elsewhere we here only present results for a slot with the dimension 46.3 x 0.1 mm. The reason for including it in this report is to illustrate the effects at electrical breakdown. The dimension of the slot is chosen in order to get a half-wave resonance at the magnetron frequency 3 GHz. At half-wave resonance we get the field enhancement necessary to initiate electrical breakdown.

In the earlier studies measurements have also been carried out on a riveted seam, which is quite similar to what can be found on an aircraft. The seam has been put to our disposal by Saab Aircraft, Linköping. We have not been able to detect any non-linear effects when irradiating this seam between 10 and 60 kV/m [13].

3.2 Corroded EMC joints

3.2.1 Joints subjected to accelerated ageing (from first SCI study)

Out of the about 40 test samples we include 5 in the present study. These 5 represent some of the most corroded object from that study. The objects are:

L5: Aluzink plate and lid, CuBe contact fingers. Corrosion test 3 (see below).
L20: Stainless steel plate and lid, carbon filled PTFE gasket, 3.2x1 mm (supplied by Gore). Corrosion test 4 (see below).
L31: As L5, but corrosion test 4 (see below).
L38: Clear chromated aluminum plate and lid, tin plated contact fingers. Corrosion test 4 (see below).
L40: Clear chromated aluminum plate and lid, silver filled elastomer. Corrosion test 4 (see below).

The corrosion tests are, a more thorough description is given in [9]:

Test 3: Damp heat, cyclic test according to IEC 62-2-28, 30 days, with addition of SO_2, 0.5 ppm and NO_2, 0.5 ppm.
Test 4: Damp heat, cyclic test according to IEC 62-2-28, 30 days, with addition of SO_2, 0.5 ppm and NO_2, 0.5 ppm, periodic immersion in 0.1 wt% NaCl solution, 30 days.

A drawing of the test objects is shown in Figure 12. Object L20 and L40 do not have plastic spacers, only one layer of paper. A photo of L38 (Clear chromated aluminum/tin plated contact fingers after exposure to test 4) is shown in Figure 13. Photos of the other four objects are shown in Appendix A and in [9].

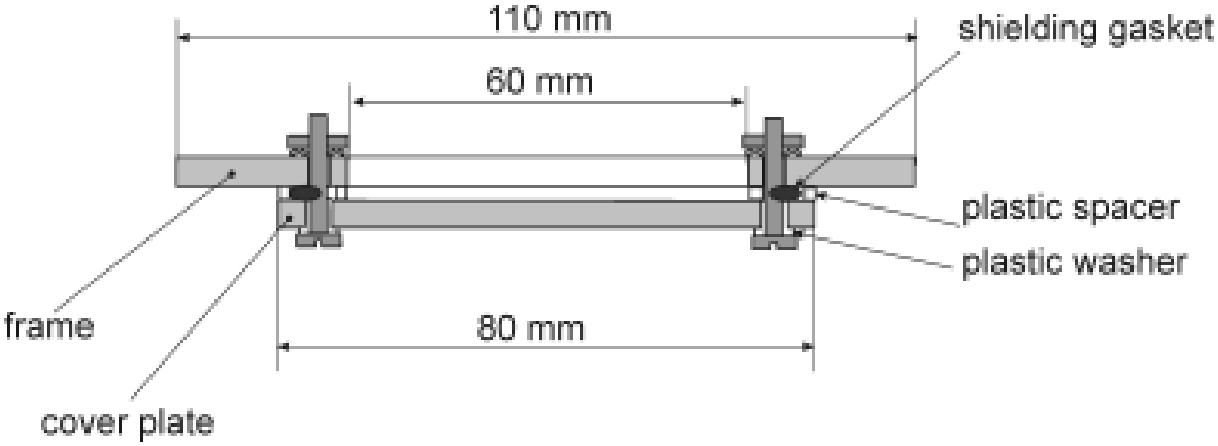

Figure 12. Geometry of the EMC joints from first study. From [9].

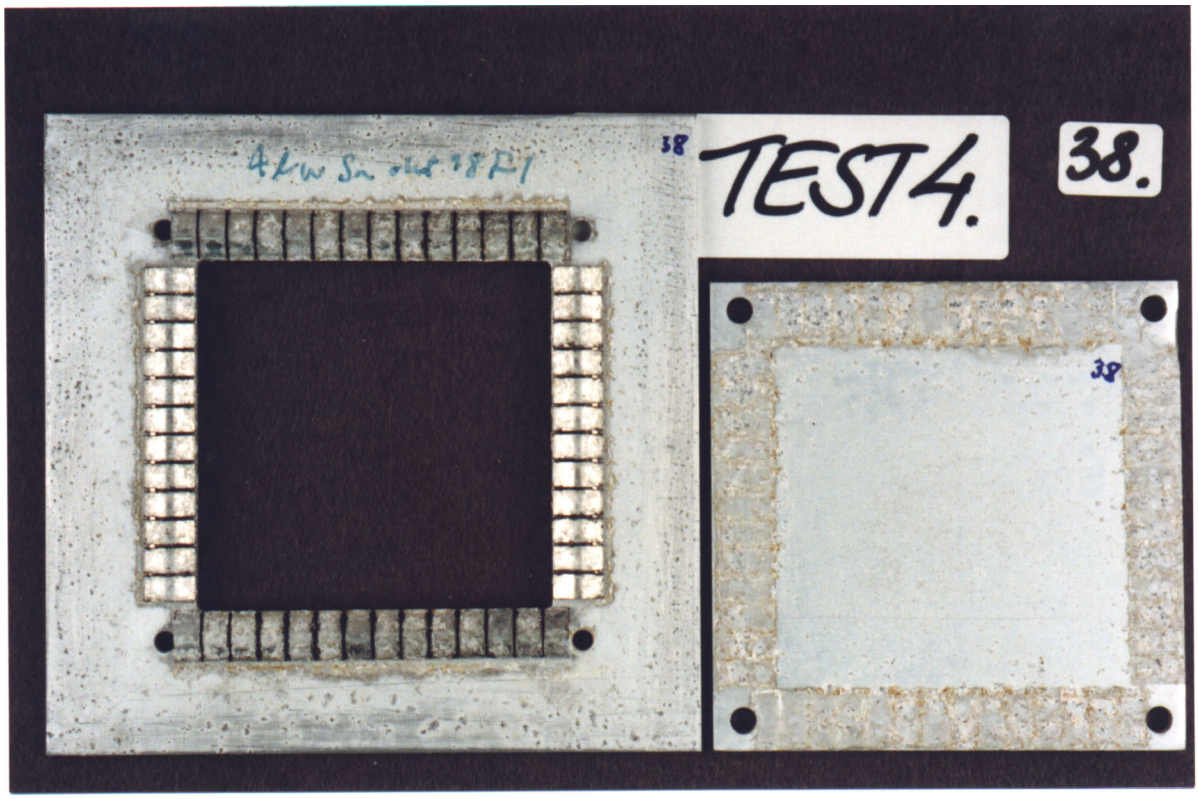

Figure 13. Object L38. Clear chromated aluminum/tin plated contact fingers after exposure to test 4 [9].

3.2.2 Joints subjected to outdoor exposure (from second SCI study)

The second KI study comprised 58 different combinations of gasket and frame and cover plate. A complete description of the objects can be found in [8]. The matrix from which the 58 combinations were made is given in Table 1 below. Each combination was made in three samples, one of them using nylon screws and two using steel screws, see Figure 14 below. In our investigation 26 objects, all with nylon screws, were chosen. The choice was made so that the 26 objects yield a representative sample of the 58 combinations. Some objects were ruled out because of the limited dynamic range of the measurements of the transmission cross section in the reverberation chamber, the cross section of these objects were just too small. All 26 objects have been demounted after the exposure and then mounted together again. The designation of the 26 objects are: C0BJ, C0CF, C0HC, C0HK, C0KC, C0LE, C1BF, C1IE, C2BF, C2EM, E0IE, E0LE, F0CF, F0GF, M0EM, M0GM, N0CF, N0FK, N0GM, N0IE, N1IE, N1IP, N3DF, N3EF, N3EM, N3IE. Six of the chosen objects showed a large change in shielding after the outdoor exposure, namely C0BJ, C0CF, M0GM, E0IE, N0IE and N3IE. The designation of the objects is defined in Table 1 below. A drawing of the geometry of the test objects is given in Figure 14. The objects have been exposed for one year, 2002-07-05 to 2003-07-28, under a hood on a terrace close to a lake, immediately north of the Stockholm city boundary (Kräftriket), see Figure 15 and [8].

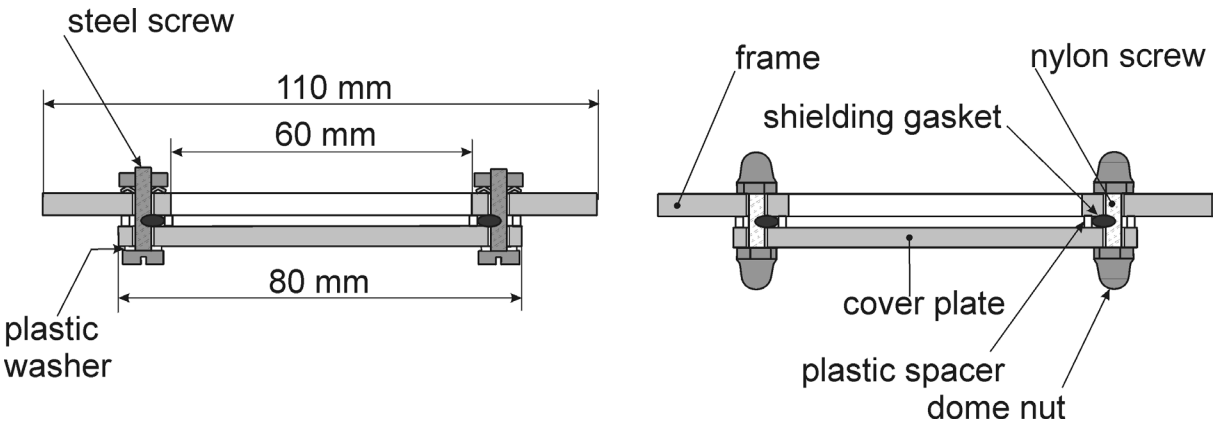

Figure 14. Geometry of EMC joints from second study. The 26 objects investigated in the present report have nylon screws (right drawing). From [8].

Figure 15. Outdoor exposure of the objects in the second study. The objects were exposed under a weather protective hood.

Table 1. Specimen designation. The letters, indicating plate and shielding gasket combination, define each test object. Example: C1BF consists of clear chromated aluminium frame and cover plates connected by a tin electroplated fingerstock shielding gasket of standard hardness.

Frame and cover plate				Shielding gasket			
metal(lic coating)		non-metallic coating		type		conductive material	
B	galvanized	0	none	B	fingerstock, standard hardness	B	zinc electroplate
C	aluminium	1	clear chromated	C	fingerstock, soft	C	aluminium
E	silver electroplate	2	yellow chromated	D	twin knitted wire mesh, no core	E	silver / silver particles
F	tin electroplate	3	ALC-coated (thin polymer)	E	double layer wire mesh with core	F	tin electroplate
M	stainless steel			F	non-resilient metal net	J	beryllium copper
N	Aluzink			G	single wire mesh in core surface	K	Monel
				H	oriented wires in foam elastomer	M	stainless steel
				I	filled silicon elastomer	P	graphite particles
				J	filled fluoro-silicon elastomer	Q	nickel+graphite particles
				K	foam core with metal foil		
				L	foam core with metal coated fabric		
				N	dispensed gasket		

4 Test Results

4.1 Generation of harmonics

When a signal with the frequency f_c is passing through a nonlinear element this may result in the production of harmonics, i.e. new frequency components will be generated having the frequencies:

$$f_n = n \cdot f_c, \quad \text{where } n = 0,2,3,4,..... \qquad (3)$$

The case $n = 0$ corresponds to what is known as envelope detection. For a CW signal this results in a DC component. For (as is the case here) an amplitude modulated signal, the envelope detection results in frequencies equal to the frequency content of the envelope of the pulse train. In our case the pulse is roughly a rectangular pulse with a length of $\tau = 1$ μs, and

the pulse repetition frequency, prf = $1/T$, is 70 Hz, i.e. $T = 14.2$ ms. The frequency content of such an envelope consists of discrete harmonics with frequencies 0, 1/T, 2/T, 3/T ,…. If we, for simplicity, assumes that the rise and fall times are zero, the magnitude of these frequency components are bounded by a $\sin(x)/x$ function where $x = \pi \cdot \tau \cdot f$. This function is approximately bounded by a constant level up to the frequency $f_{bp} = 1/\pi\tau = 318\,\text{kHz}$. (The magnitude of the DC component is half that of the other components.) Above f_{bp} the frequency components are bounded by a slope falling 20 dB/decade, see e.g. [10, pp.363]. In practice, we normally use a sampling rate of 20 GHz and a time window equal to 4 μs (or sometimes 2 μs), i.e. the number of samples for one pulse is 80 000 (or 40 000). In the present study we have, except for the thin slot, used a time window of 4 μs and 80 000 samples. This means that the lowest frequency components resulting from an FFT analysis are equal to 0, 0.25, 0.5, 0.75, .. MHz. Thus, if envelope detection exists this should be seen only for a few of the lowest frequency components. It shall be noted that the real pulses deviate quite strongly from the ideal rectangular pulse described above. The aim of the discussion above is only to point out the general features that are expected.

For an aperture that is symmetric with respect to the applied electric filed we expect only frequency components corresponding to $n = 3,5,7,...$. For an asymmetric aperture we expect also frequency components corresponding to $n = 0,2,4,...$. This can be understood by noting that in the symmetric case the current-voltage relation can be written as:

$$I = f(V) = a \cdot V + b \cdot V^3 + c \cdot V^5 + d \cdot V^7 + ... \qquad (4)$$

i.e. f can be expressed as a power series only including odd powers of V. The reason being that a change of just the polarity of the voltage (the electric field) should also result in a change of the polarity of the current, the magnitude being unchanged. Since the slot geometry is (as far as we can control) symmetric we expect not to see any 6 GHz component but possibly a 9 GHz component (the sampling rate does not permit us to see higher orders of harmonics). On the other hand, the EMC joints are not expected to be highly symmetric since different materials are combined (and since the corrosion process is, we expect, to some extent random with respect to geometry).

As was mentioned above the appearance of a substantial low frequency content, caused by envelope detection of the pulsed microwave signal, would probably be of most interest. The reason is that electronic equipment is usually more susceptible to frequencies below microwave frequencies. However, as was mentioned in paragraph 2.3.1, and which will also be discussed below, the low sensitivity of the D-dot probe at low frequencies makes it hard to draw any certain conclusions concerning the magnitude of the envelope detection.

4.2 Reduction in transmitted power

As already mentioned an electrical breakdown typically leads to a reduction of the energy transmitted through the aperture. For, e.g., a half-wave resonant slot a discharge in the middle of the slot creates a short circuit of the slot. By that two non-resonant slots replace the former resonant slot. This leads to a reduction in the total transmission cross section of the slots. For a half-wave resonant thin slot it holds that the transmission cross section, its dimension is square meter, is equal to [14]:

$$\sigma_{a,0} = 2 \cdot \frac{\lambda^2}{4\pi} \cdot D = 0.26 \cdot \lambda^2 \qquad (5)$$

where D is the directivity, $D = 1.64$, For the frequency 3 GHz, i.e. $\lambda = 0.1$, we get: $\sigma_{a,0} \approx 0.0026 = -26$ dBsm (dBsm="decibel square meter"). We are here considering normal incidence and strong coupling, i.e. the electric field perpendicular to the slot. Equation (5) showed an excellent agreement with Finite-Difference Time-Domain (FDTD) calculations of a slot, and a rather good, within 3 dB, agreement with measurements carried out in FOI large anechoic chamber, see [14]. If the resonant slot is short-circuited in the middle two non-resonant slots are created. Each one of these has a transmission cross-section of roughly 24-25 dB (FDTD simulations), or 27-28 dB (measurement), below the first resonance peak. This can be derived from Figure 9 in [14]. Thus, when electrical breakdown is initiated, assuming that the breakdown causes a short circuit in the middle of the slot, we expect the total transmission cross section to decrease by roughly 21-25 dB. We here assume that the transmission cross section of the two slots is roughly equal to the sum of the two individual slots. As will be seen in paragraph 4.6 this is in very good agreement with the measured results.

The abrupt change in the transmitted power results in a frequency broadening of the spectral content of the pulse. This can easily be understood in analogy with what was described in paragraph 4.1. In the present case the 3 GHz microwave signal is amplitude modulated by an (approximately) square pulse having a length of $\tau = 1$ μs. This amplitude modulation gives, in the frequency spectrum, a broadening of the spectrum around 3 GHz. The width, defined as the breakpoint between the slope of the envelope of 0 dB and the slope –20 dB per decade, of the pulse in the frequency spectrum, cf. paragraph 4.1 above, equals $2 \cdot f_{bp} = 2/\pi\tau = 636$ kHz. If we instead look at the zeros of the main lobe of the $\sin(x)/x$ function we get a width, around 3 GHz, of the main lobe equal to $2/\tau = 2$ MHz [10]. For a short pulse, say 10 ns, we get corresponding widths of 63.6 MHz and 200 MHz, respectively. Again, it should be remarked that the real pulses do not look like the ideal pulse described here, see the results below, the discussion here just aim to illustrate the general behaviour between pulse length and frequency content.

4.3 Magnetron pulse characteristics

The shape of the magnetron pulse, measured in the wave-guide, varies slightly between pulses. An example of the pulse, in the time-domain, is shown in Figure 16. The frequency spectrum, obtained by applying the MATLAB FFT, of the same pulse is shown in Figure 17. In this case, contrary from the measurements below using the D-dot probe, we just apply the FFT on the voltage signal from the probe in the wave-guide. As can be derived from the spectrum the peak value of the 6 GHz component is about 36 dB below the peak value of the main peak at 3 GHz. A measurement of 10 spectra shows yields the value 35.6 ± 0.6 dB. The corresponding pulses in time-domain are shown in Appendix B.

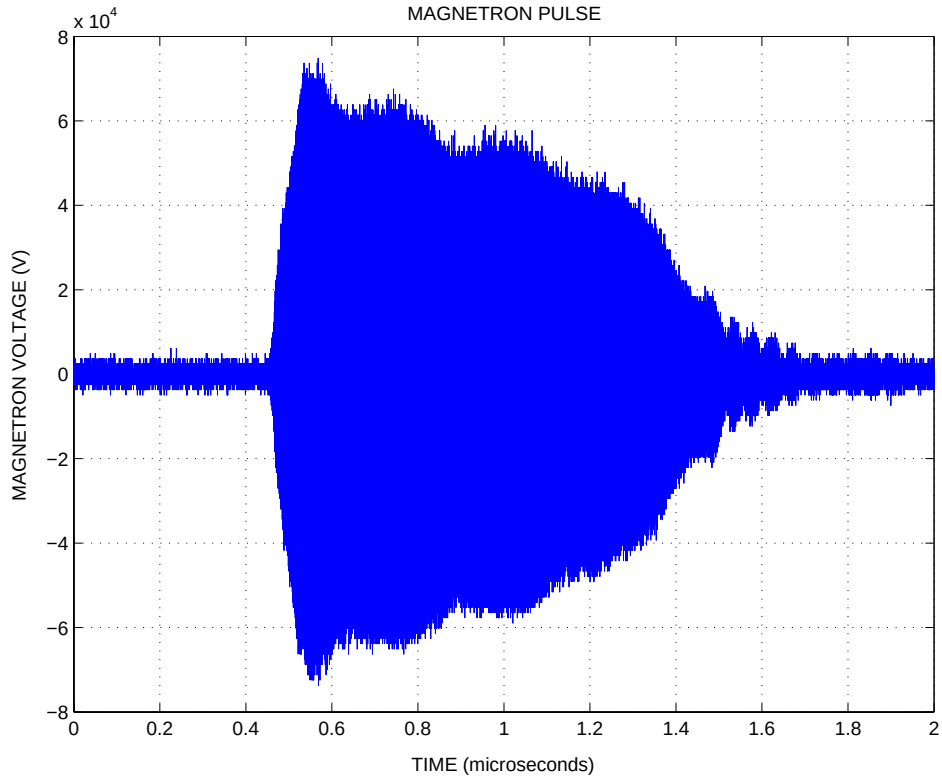

Figure 16. Pulse from magnetron measured in the reference port. Time-domain. UL_100_040112, first pulse.

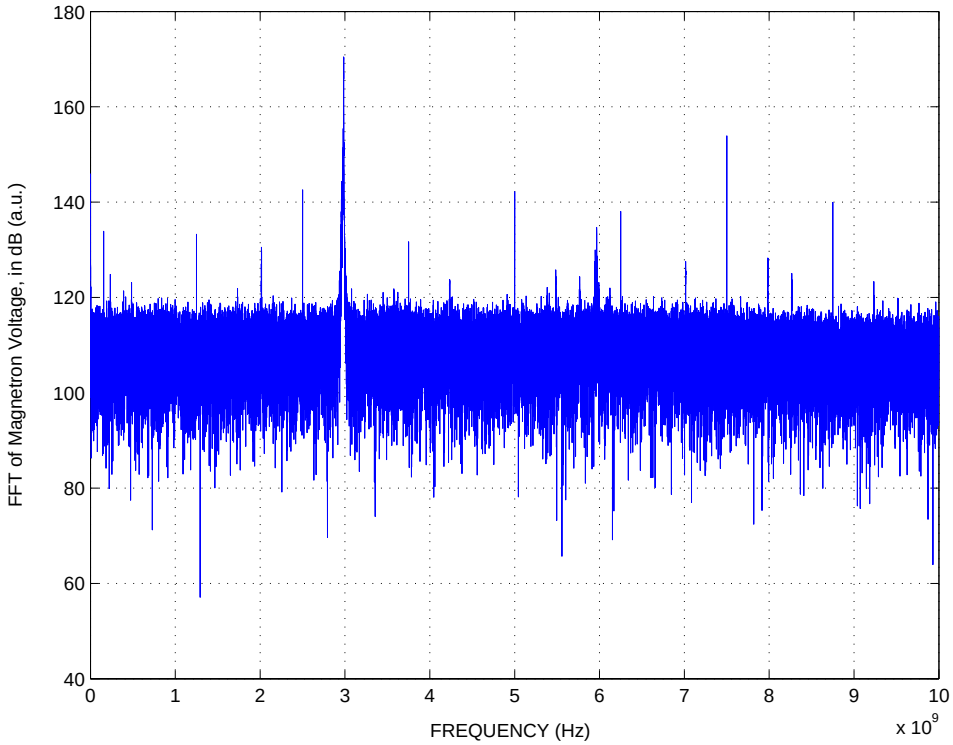

Figure 17a. Pulse from magnetron measured in reference port. Frequency-domain, between 0 and 10 GHz. UL_100_040112, first pulse.

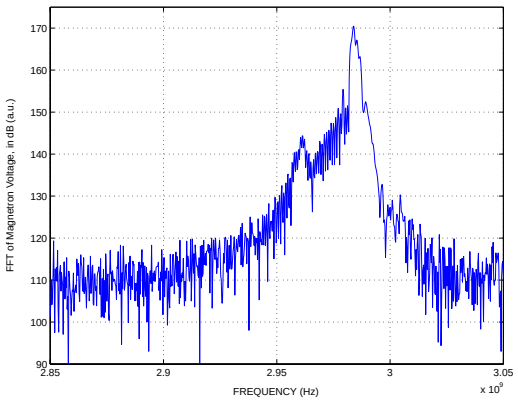

Figure 17b. Pulse from magnetron measured in reference port. Frequency-domain, between 2.85 and 3.05 GHz.

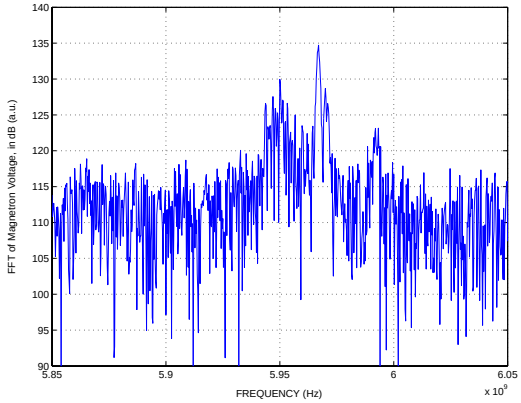

Figure 17c. Pulse from magnetron measured in reference port. Frequency-domain, between 5.85 and 6.05 GHz.

As can be seen in the spectrum in Figure 17a there are sharp spikes, obviously artifacts, at 1.25, 2.5, 3.75, …10 GHz, i.e. at frequencies corresponding to 20 GHz multiplied by $n/16$, where *n=1, 2, 3, ... 8.* The same phenomenon was reported in another FOI study [15, p.24 and 28]. The spikes were presumed to have their origin in the digital circuits controlling the digital memory. The other peaks (apart from the genuine peaks at 3 and 6 GHz), which are broader, can be derived from a mixing between the genuine peaks at 3 and 6 GHz and these artifacts. (There seem however to be a genuine peak also at 3.575 GHz for which we have no explanation).

4.4 The reference case: open hatch

It was noticed during the field calibration that the 6 GHz component extracted from the magnetron wave guide does not turn up with the same magnitude (relative to the magnitude of the 3 GHz peak) when it was measured by the D-dot probe at the location of the aperture under test (with the test box being removed). This reflects that the antenna pattern for the transmit antenna is significantly different for 3 and 6 GHz. Therefore, in order to have a reference spectrum to compare with, measurements were carried out with the 29x29 cm hatch open. In the time-domain one can hardly see any difference, see Figure 18, but the corresponding spectrum, see Figure 19, shows a much less pronounce peak at 6 GHz. The spectrum in Figure 19a clearly illustrates the $1/f$ dependence of the background level due to the compensation for the probe's derivative nature, cf. paragraph 2.3.1 above. The 6 GHz peak is 51.5±1.2 dB below the 3 GHz peak at 100 mm distance, 51.3±1.5 dB at 200 mm (the 6 GHz peaks are however rather weak), 52.6±1.3 dB at 500 mm, 53.3±0.9 dB at 1000 mm (the 6 GHz peaks are also in this case rather weak) and 50.5±0.6 dB at 2000 mm. When we look for a 6 GHz peak as an indication of non-linear effects we therefore compare that spectrum with the spectrum from the open hatch experiment (i.e. not with the spectrum of the pulse measured in the wave-guide).

The spectrum around 0 Hz can be found in Appendix C. As can be seen in that figure, as well as in Figure 19a, the *1/f*-compensation of the frequency domain data yields a higher background level at 0.25 MHz (the lowest frequency in the plots) than the peak level at 3 GHz. The difference for the open hatch is 40 dB. This means that only very powerful low frequency components can be revealed. This problem will be further discussed in connection to the presentation of the results below.

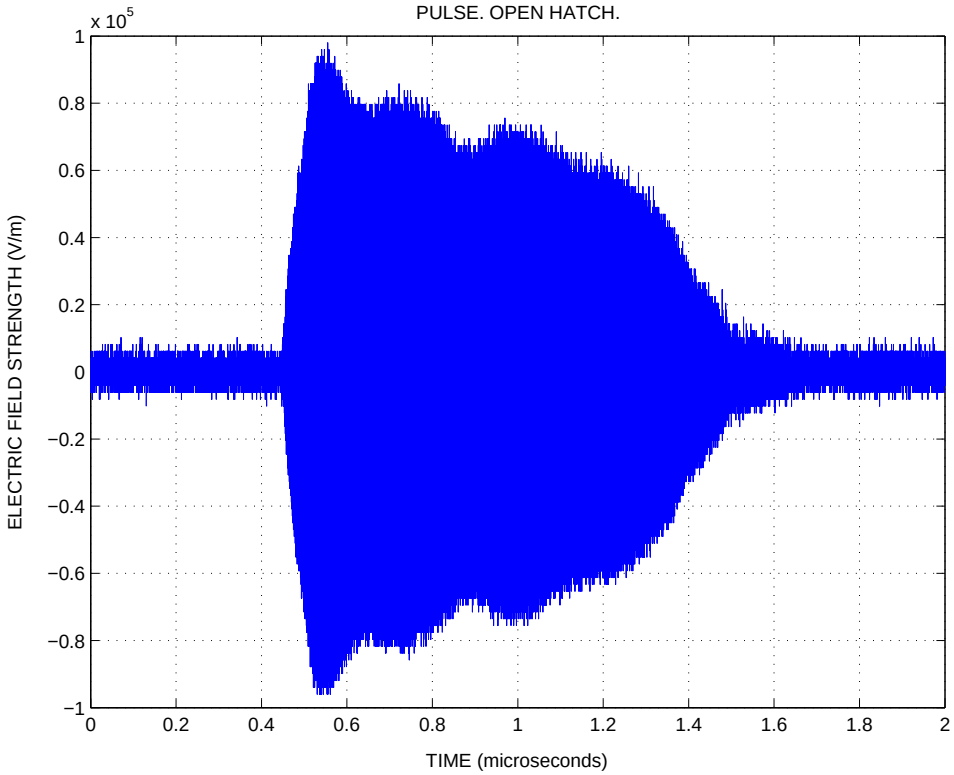

Figure 18. Pulse measured in the test box with hatch open. Distance 100 mm. E = 53 kV/m. Time-domain. UL_100_040112, first pulse.

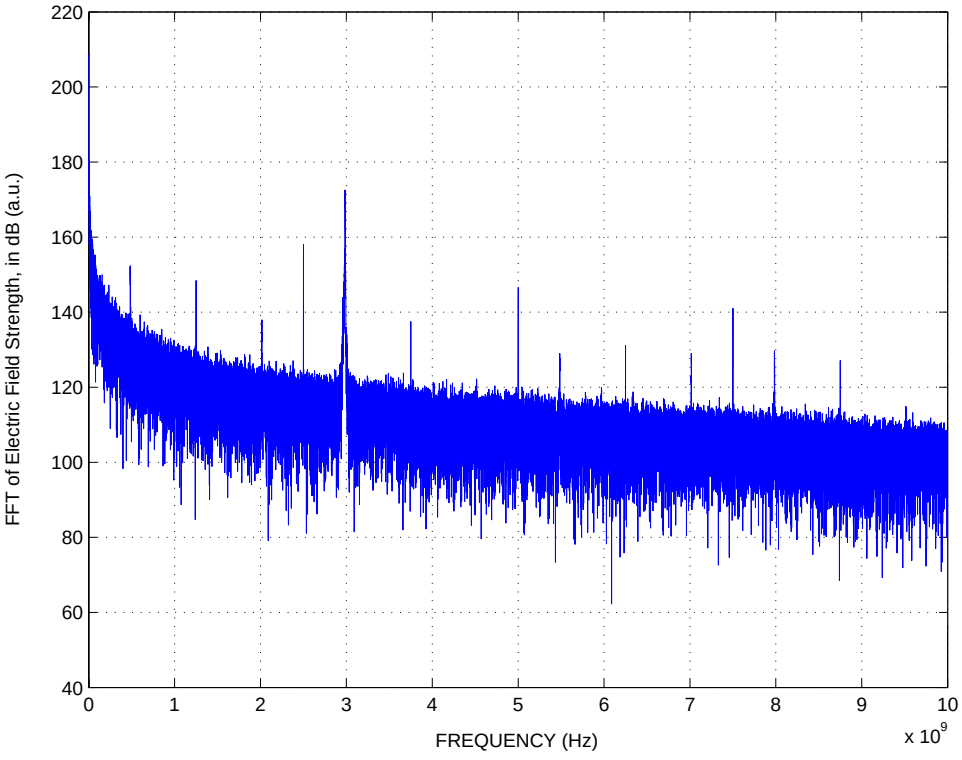

Figure 19a. Pulse measured in test box with hatch open. Distance 100 mm. E = 53 kV/m. Frequency-domain, between 0 and 10 GHz. UL_100_040112, first pulse.

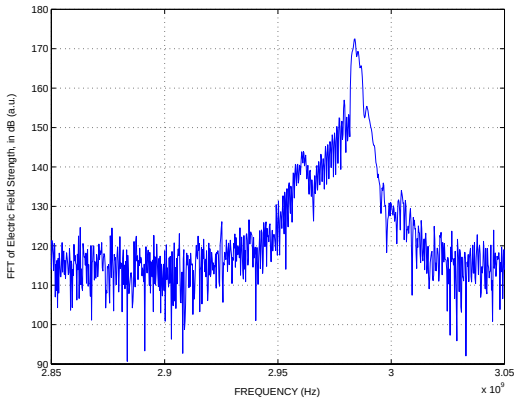

Figure 19b. Pulse measured in test box with hatch open. Distance 100 mm. E = 53 kV/m. Frequency-domain, between 2.85 and 3.05 GHz. UL_100_040112, first pulse.

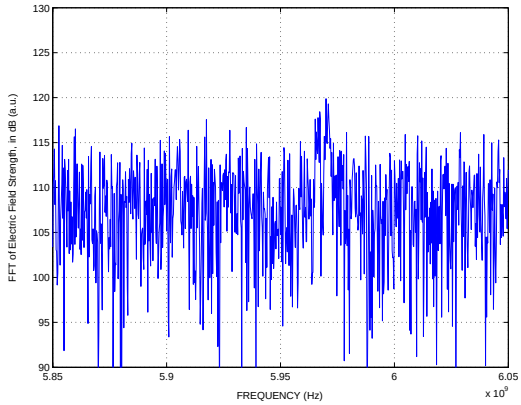

Figure 19c. Pulse measured in test box with hatch open. Distance 100 mm. E = 53 kV/m. Frequency-domain, between 5.85 and 6.05 GHz. UL_100_040112, first pulse.

4.5 Background level. Closed hatch.

When the AUTs where replaced by a solid plate almost no signal at all could be detected. This assures that the detected signals in the actual tests really have their origin in leakage through the AUT's and are not caused by leakage between the surfaces connecting the AUTs to the flanges of the test setup.

A time domain plot of a result at 500 mm distance, which was the only distance for which a signal (at one occasion) could be detected at all, is shown in Figure 20. The corresponding frequency domain plot is shown in Figure 21.

The spectra around 0 Hz, 3 GHz and 6 GHz can be found in Appendix C.

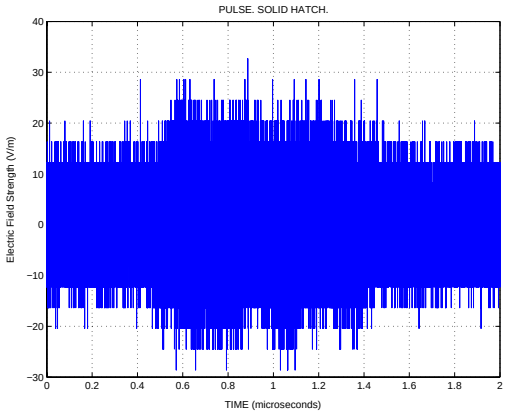

Figure 20. Pulse measured in test box with solid hatch. Distance 500 mm. Time-domain. Solid_pytte_06_500_050225, first pulse.

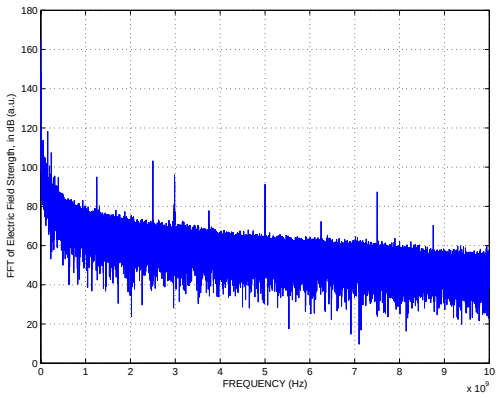

Figure 21. Pulse measured in test box with solid hatch. Distance 500 mm. Frequency-domain, between 0 and 10 GHz. Solid_pytte_06_500_050225, first pulse.

4.6 Thin slot. Results

The thin slot, 46.3 x 0.1 mm, was irradiated at the distances 100 mm (around 52 kV/m), 200 mm (37 kV/m), 300 mm (28 kV/m), 400 mm (24 kV/m), 500 mm (20 kV/m), 600 mm (18 kV/m), 800 mm (15 kV/m), 1000 mm (12 kV/m) and 1200 mm (10 kV/m). The electric field strength is given in parenthesis. At 100 mm distance 10 runs were performed. This gave a standard deviation in the measured field strength of 0.8 kV/m.

At 800 mm distance there were no electrical breakdown registered out of 50 runs. At 600 mm there were 10 electrical breakdowns out of 100 runs. The measured electric field strength was $E = 18.2 \pm 0.3$ kV/m where ±0.3 denotes the standard deviation for 10 pulses. At a distance of 500 mm ($E = 20$ kV/m) and shorter, electrical discharges always occurred. Figure 22 shows an example of a transmitted pulse at the distance 100 mm, where $E = 52$ kV/m. Electrical breakdown takes place after about 10 ns. An analysis of 100 runs at 100 mm distance yields a breakdown time of 11.6 ± 3.6 ns. As was noted above, the transmitted field was, for the thin slot, measured by use of a horn antenna mounted behind the slot (i.e. not by use of the D-dot probe).

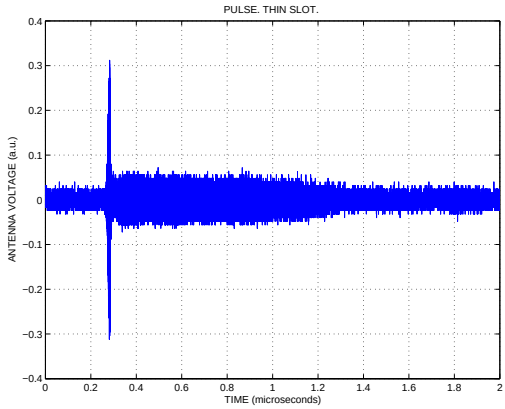

Figure 22a. Pulse transmitted through the 46.3 x 0.1 mm slot measured using a horn antenna. Distance 100 mm. $E = 52$ kV/m. Time domain. S5_a100_1_030311.

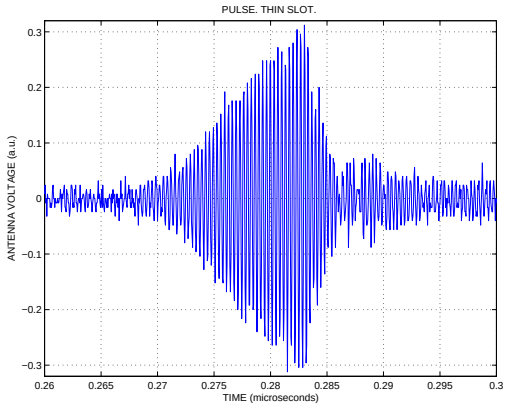

Figure 22b. Pulse transmitted through the 46.3 x 0.1 mm slot measured using a horn antenna. Distance 100 mm. $E = 52$ kV/m. Time domain. Increased time resolution. S5_a100_1_030311.

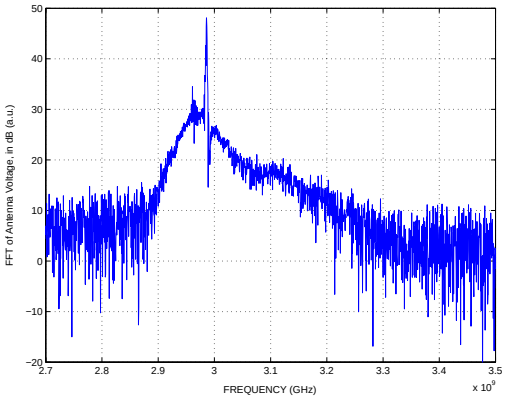

Figure 23a. Pulse transmitted through the 46.3 x 0.1 mm slot. Distance 100 mm. $E = 52$ kV/m. Frequency domain, between 2.7 and 3.5 GHz. S5_a100_1_030311.

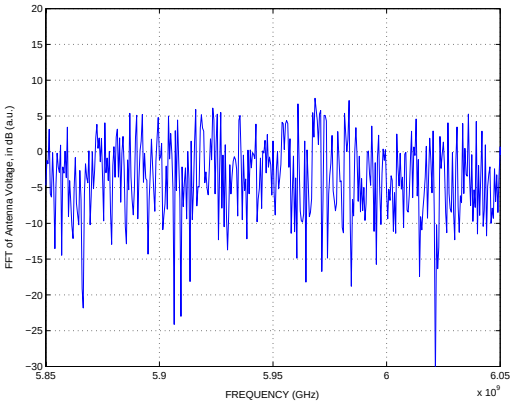

Figure 23b. Pulse transmitted through the 46.3 x 0.1 mm slot. Distance 100 mm. $E = 52$ kV/m. Frequency domain, between 5.85 and 6.05 GHz. S5_a100_1_030311.

A frequency analysis around 3 GHz of a transmitted pulse is shown in Figure 23a. The corresponding frequency plot around 6 GHz is shown in Figure 23b. As can be seen there is no peak is visible at 6 GHz. Since the slot has a symmetric geometry along the direction of the electric field it is not expected to have a strong peak at 6 GHz, cf. the discussion in paragraph 4.1. There is, however, neither any peak at 9 GHz, contrary to what could have been expected from the discussion in paragraph 4.1, see Appendix C. Out of 100 pulses studied at 100 mm distance we could not detect any peak at 9 GHz (files named s5_a100_1_030311, s5_a100_2_030311, …, s5_a100_10_030311). Furthermore, we see a broadening of the pulse spectrum around 3 GHz, see Figure 23a, which is, at least qualitatively, in accordance with the discussion in paragraph 4.2. In fact, if one makes an analysis of the spectral content of a triangular pulse, which is a far much better description of the transmitted pulse in Figure 22 than (as in paragraph 4.2) using a rectangular pulse, the fit between theoretical and measured data becomes good [11; pp. 51].

The reduction in transmitted power at 100 mm distance is, within about one dB, 25 dB [11; Figure A4, series s1 and s5]. This is in excellent agreement with the estimate from FDTD simulations, and in reasonable agreement with the measurement reported in [14], cf. also paragraph 4.2. The reduction in transmitted energy depends on the time to breakdown, for the case considered here (breakdown time around 12 ns, the transmitted energy reduction is about 24 dB [11; Figure A9, series s1 and s5].

In Appendix C we also show the complete spectrum, the spectrum close to 0 Hz and that around 9 GHz.

4.7 Joints subjected to accelerated ageing. Results.

4.7.1 Transmission cross section in reverberation chamber

In order to evaluate possible damage or degradation of the shielding joints the cross-sections were measured both before and after exposure to the high field levels. The measured transmission cross-sections before and after the high-level radiation are shown in Figure 24. In the figure two reference curves are included. The upper curve shows the transmission cross section for a 30 mm diameter circular hole. This was used as a reference for deriving the absolute values of the transmission cross sections of the test objects, cf. paragraph 2.2. A solid hatch, the lower red curve, has been used to establish the measurement floor, i.e. it shows the cross section corresponding the unwanted leakage around the edges of the test objects. A plot of the differences is shown in Figure 25. As can be seen in the plot it is difficult to see any systematic changes after the irradiation. The differences for the test objects are not greater than the variation for the solid hatch (which has not been subjected to any high level irradiation). This conclusion holds also for object 38, which is the only object for which a distinct non-linear process could be detected (that happened only in one of the runs), see next paragraph.

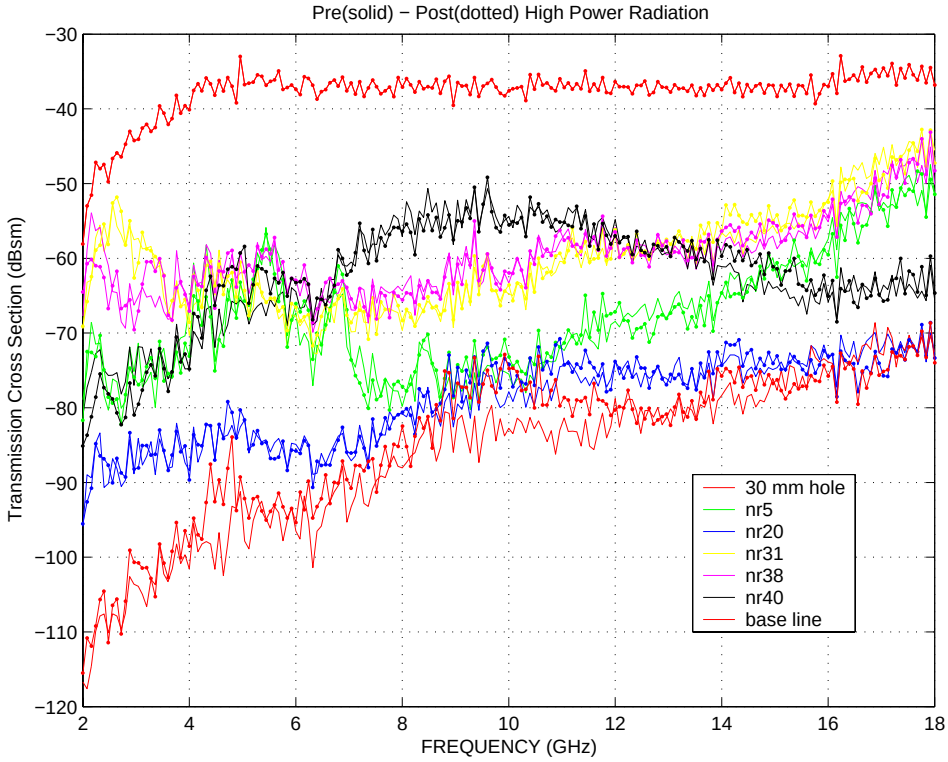

Figure 24. Transmission Cross Section of the five test objects subjected to accelerated ageing measured before and after the exposure to the high field levels. The upper curve, 30 mm hole, is included for reference. The lower curve (red) is measured using a solid hatch.

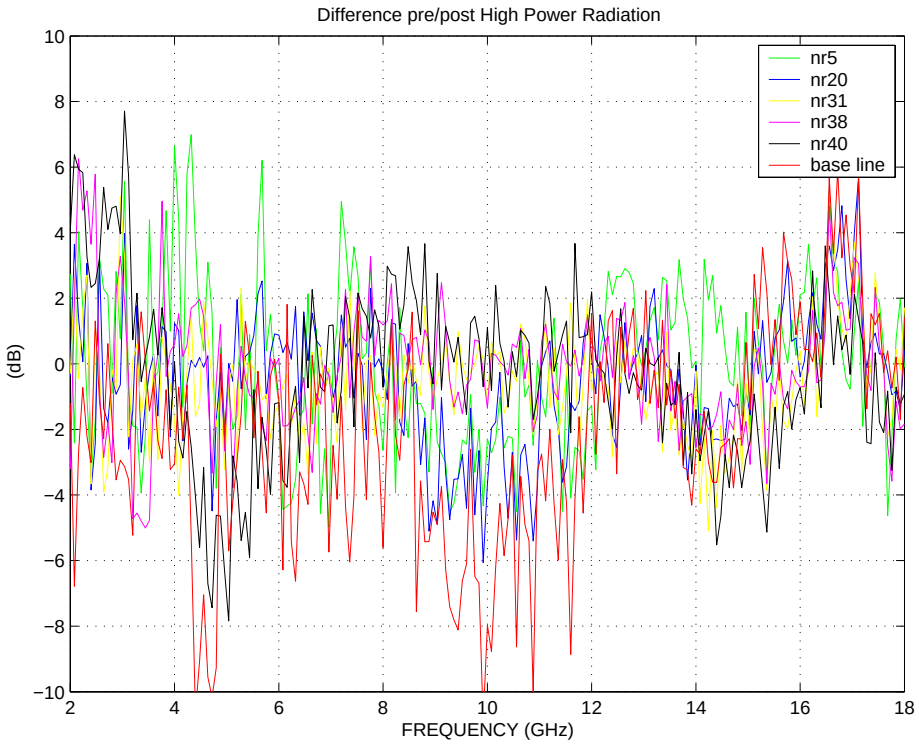

Figure 25. The difference between before and after high level irradiation for the curves shown in Figure 24 (30 mm hole not included).

4.7.2 High-level testing

The tests were performed at 100, 200, 500 and 1000 mm distance. Except for test object L38, where (mostly only weak) non-linear effects are seen at all test distances and a pronounced effect is seen in one case (see below) non-linear effects are hardly noticeable. The indications of non-linear effects are here defined by noticeable changes in the time domain shape of the pulse, and/or the occurrence of peaks at 6 GHz, and/or the occurrence of low frequency content, the latter presumably due to envelope detection. The problem regarding the difficulty to detect envelope detection will be discussed below. There are also some noticeable, but small effects, for L31 for the distances 100, 200 and 500 mm. In general, if there are peaks at all at 6 GHz they are usually very small and look similar to those visible for open hatch i.e. they are slightly more than 50 dB below the peak level at 3 GHz. A typical plot for L38 at 200 mm distance in the time- and frequency domain around 6 GHz is shown in Figure 26a. The corresponding frequency spectrum around 6 GHz is shown in Figure 26b, around 0 GHz in Figure 26c, and around 3 GHz in Figure 26d. In Appendix D we include time domain plots and the corresponding spectra around 6 GHz for the all the 10 measurements for L38 carried out at 200 mm distance. The peak levels at 6 GHz where –51.8 dB ±0.9 below the peak level at 3 GHz. At least for pulse 1 also a low frequency content can be seen, se Figure D3 in Appendix D.

None of the five test objects show any peaks at 9 GHz. The detected electric field strength of the transmitted signal varied, at 200 mm distance, from around 80 V/m for test object L20, 130 V/m for L5, 180 V/m for L40, to around 1 kV/m for L31 and L38.

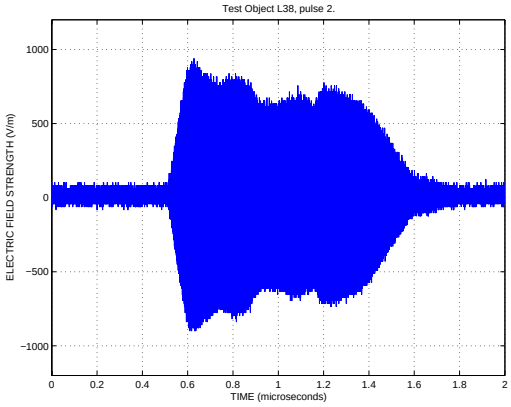

Figure 26a. Pulse transmitted through test object L38. Distance 200 mm. Pulse 2. E = 38 kV/m. Time Domain.
L38_200_031218.

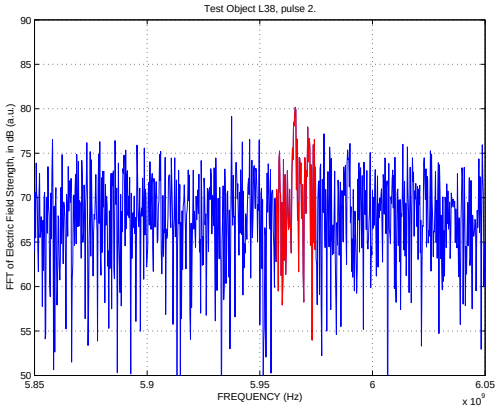

Figure 26b. Pulse transmitted through test object L38. Distance 200 mm. Pulse 2. E = 38 kV/m. Frequency Domain, between 5.85 and 6.05 GHz. The expected location of the peak is denoted by red colour. L38_200_031218.

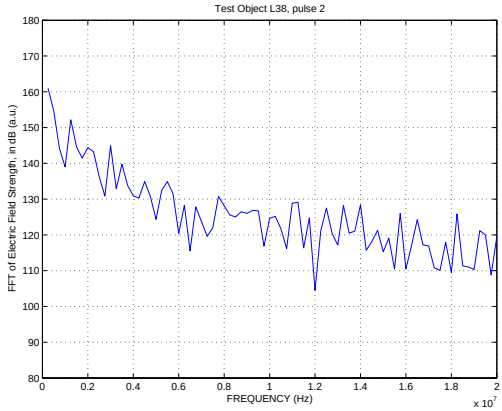

Figure 26c. Pulse transmitted through test object L38. Distance 200 mm. Pulse 2. E = 38 kV/m. Frequency Domain, between 0 and 20 MHz.
L38_200_031218.

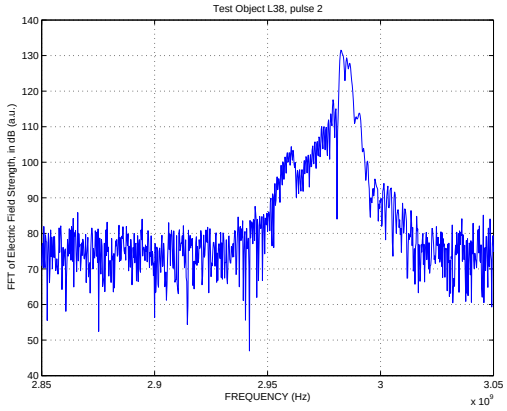

Figure 26d. Pulse transmitted through test object L38. Distance 200 mm. Pulse 2. E = 38 kV/m. Frequency Domain, between 2.85 and 3.05 GHz.
L38_200_031218.

However, it is interesting to note that in one case, object 38, distance 500 mm, pulse 1, there is a marked distortion of the pulse in the time domain, see Figure 27a. (It shall be reminded that the existence of strong non-linear effects means that the calibration factor used in the time domain plots may not be exactly correct, see paragraph 2.3.1.). The frequency plot around 6 GHz is shown in Figure 27b. The peak at 6 GHz is only 44.6 dB below the peak at 3 GHz. The frequency plot around 0 Hz is shown in Figure 27c and the plot around 3 GHz in Figure 27d. It is clearly seen that the plot around 0 Hz shows a much stronger variation with frequency, i.e. the slope is steeper, compared to the other cases (see e.g. the plots for the open and closed hatch in Appendix C). In Appendix D we present plots using a logarithmic frequency scale. This makes it easier to distinguish between the 20 dB per decade slope that has its origin in the compensation for the 1/f-dependence of the D-dot probe, making a 20 dB/decade slope of the background level, and a genuine envelope detection. In those plots one can clearly notice a difference between the distorted pulse for object 38 (distance 500 mm, pulse 1) and the other pulses. In most of the latter cases there is a steady 20 dB per decade slope all the way down to 0 Hz. This is not the case for object 38, pulse 1, at the distance 500 mm, where we can see a shift in the slope towards lower frequencies. Also L38, pulse 1, at 200 mm shows this behavior although less pronounced. As can be seen in Figure 27 (and in Appendix D) the amplitude of the frequency spectrum for L38 (pulse 1) at 200 mm distance at 0.25 MHz is about 65 dB higher than the amplitude for the 3 GHz peak. Although the peak at 3 GHz is much broader it indicates that a lot of energy may have been shifted towards lower frequencies. Some preliminary analyses based on an integration of the time domain data (the D-dot probe is derivative) indicate that the level of the signal due to envelope detection may even be larger than the 3 GHz signal. These conclusions are however very uncertain and the matter should be further evaluated in the future. As noted earlier the uncertainty of the analysis of the low frequency content is due to the low sensitivity of the D-dot probe at low frequencies.

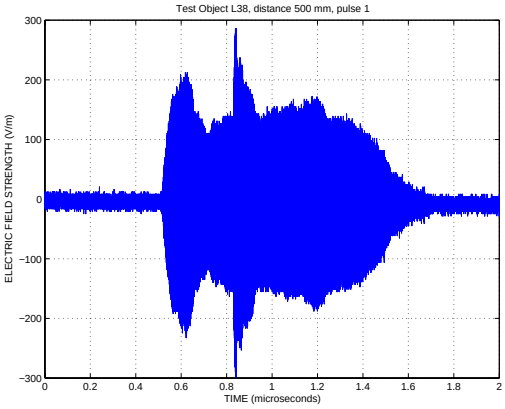

Figure 27a. Pulse transmitted through test object L38. Distance 500 mm. Pulse 1. E= 21 kV/m. Time Domain.
L38_500_031218.

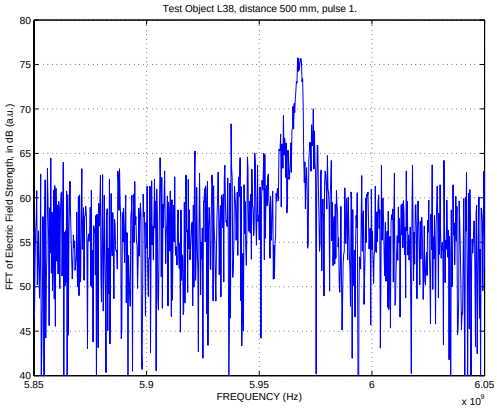

Figure 27b. Pulse transmitted through test object L38. Distance 500 mm. Pulse 1. E = 21 kV/m. Frequency Domain, between 5.85 and 6.05 GHz.
L38_500_031218.

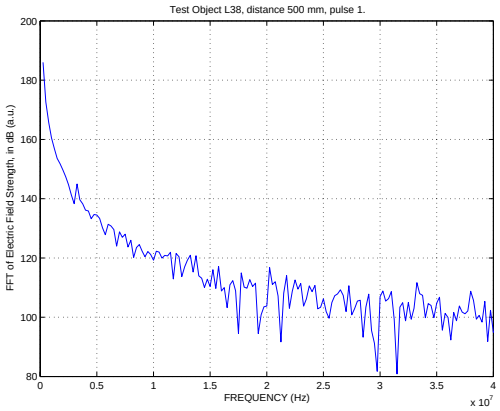

Figure 27c. Pulse transmitted through test object L38. Distance 500 mm. Pulse 1. E = 21 kV/m. Frequency Domain, between 0 and 40 MHz.
L38_500_031218.

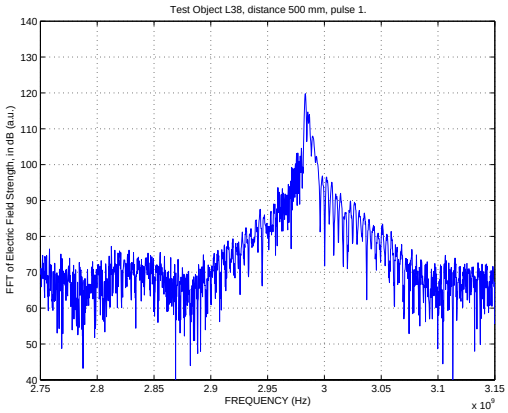

Figure 27d. Pulse transmitted through test object L38. Distance 500 mm. Pulse 1. E = 21 kV/m. Frequency Domain, between 2.75 and 3.15 GHz.
L38_500_031218.

4.8 Joints subjected to outdoor exposure. Results.

4.8.1 Transmission cross section in reverberation chamber

In order to evaluate possible damage or degradation of the 26 shielding joints the cross-sections were measured both before and after exposure to the high field levels. The measured transmission cross-sections before and after the high-level radiation are shown in Figure 28 - 32. Again a solid hatch has been used to establish the measurement floor, i.e. it shows the cross section corresponding the unwanted leakage around the edges of the test objects. Plots of the differences are also shown in Figure 28 - 32. As can be seen in these plots it is difficult to see any systematic changes after the irradiation. The differences for the test objects are usually not greater than the variation for the solid hatch (which has not been subjected to high level irradiation). The six objects, C0BJ, C0CF, M0GM, E0IE, N0IE and N3IE, which showed the greatest change in shielding after exposure (cf. paragraph 3.2.2) show somewhat larger deviations after exposure (although the effect is not large).

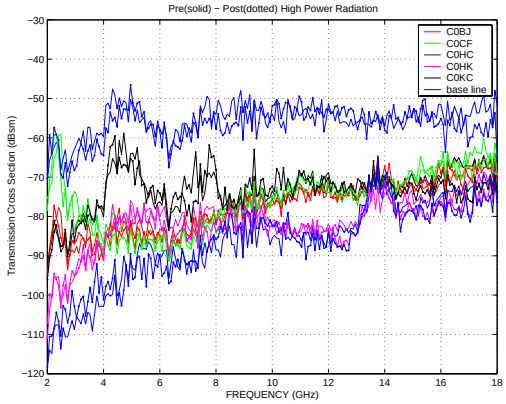

Figure 28a. Transmission Cross Section of five test objects, C0BJ, C0CF, C0HC, C0HK and C0KC, subjected to outdoor exposure measured before and after the exposure to the high field levels. The lower curve (base line) is measured using a solid hatch.

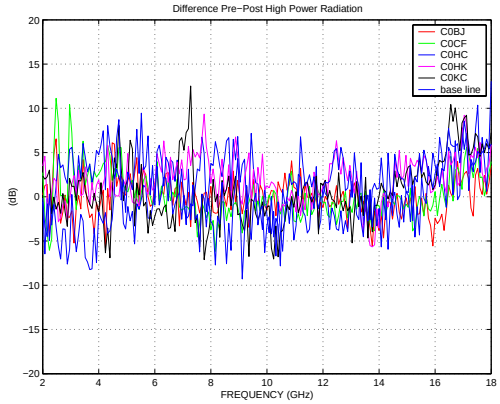

Figure 28b. The difference between before and after high level irradiation for the curves shown in Figure 28a.

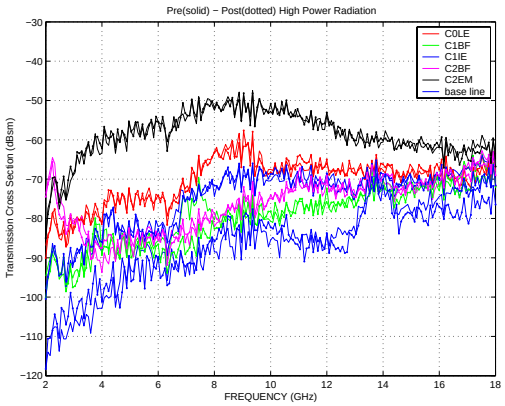

Figure 29a. Transmission Cross Section of five test objects, C0LE, C1BF, C1IE, C2BF and C2EM, subjected to outdoor exposure measured before and after the exposure to the high field levels. The lower curve (base line) is measured using a solid hatch.

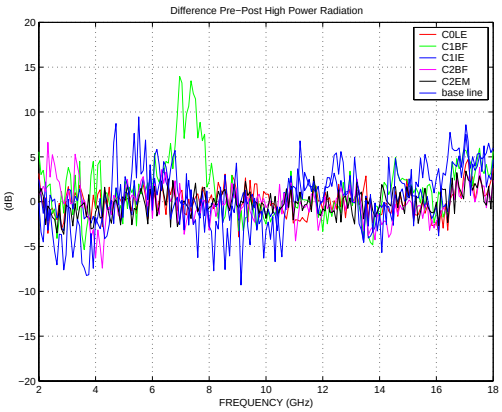

Figure 29b. The difference between before and after high level irradiation for the curves shown in Figure 29a.

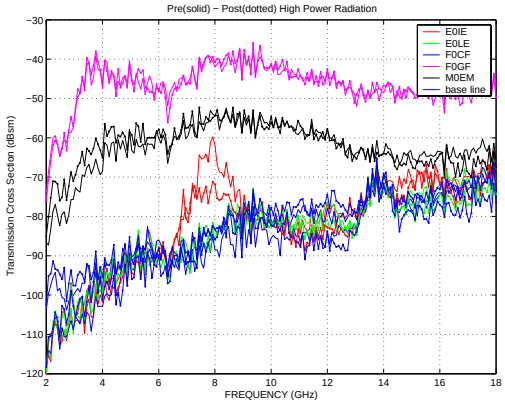

Figure 30a. Transmission Cross Section of five test objects, E0IE, E0LE, F0CF, F0GF and M0EM, subjected to outdoor exposure measured before and after the exposure to the high field levels. The lower curve (base line) is measured using a solid hatch.

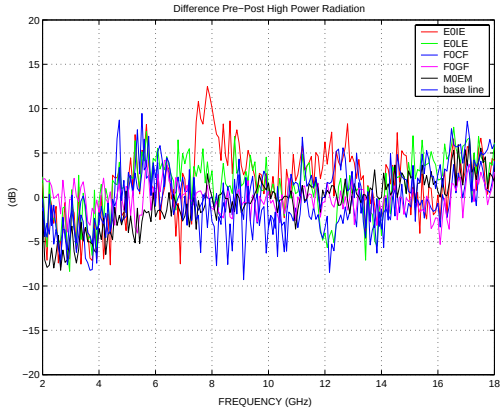

Figure 30b. The difference between before and after high-level irradiation for the curves shown in Figure 30a.

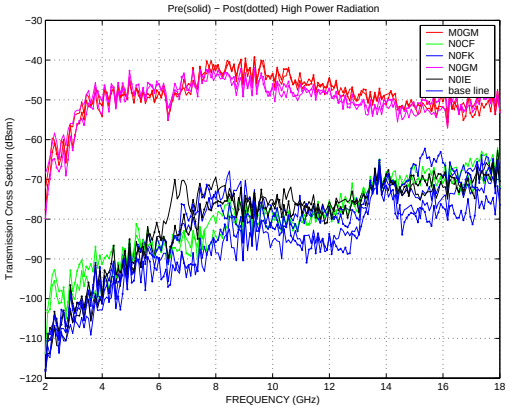

Figure 31a. Transmission Cross Section of five test objects, M0GM, N0CF, N0FK, N0GM and N0IE, subjected to outdoor exposure measured before and after the exposure to the high field levels. The lower curve (base line) is measured using a solid hatch.

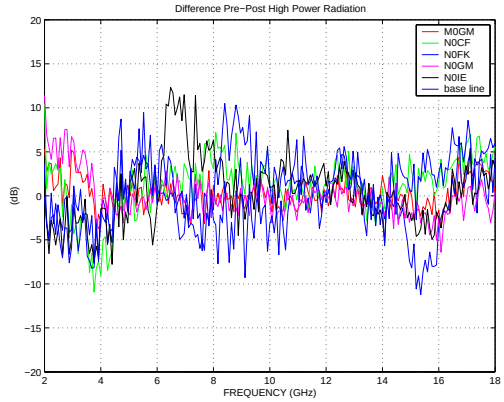

Figure 31b. The difference between before and after high-level irradiation for the curves shown in Figure 31a.

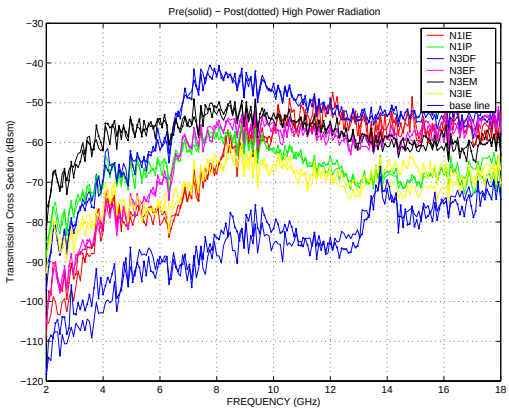

Figure 32a. Transmission Cross Section of six test objects, N1IE, N1IP, N3DF, N3EF, N3EM and N3IE, subjected to outdoor exposure measured before and after the exposure to the high field levels. The lower curve (base line) is measured using a solid hatch.

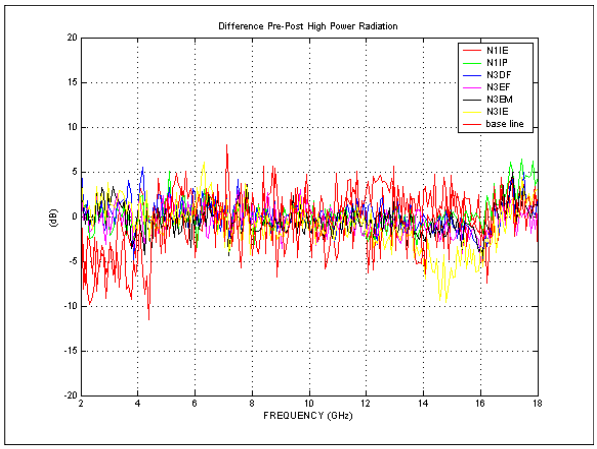

Figure 32b. The difference between before and after high-level irradiation for the curves shown in Figure 32a.

4.8.2 High level testing

The tests were performed at 200, 500 and 1000 mm distance. Only 9 of the objects (C0HC, C2EM, F0GF, M0GM, N0GM, N1IP, N3DF, N3EM and N3IE) showed levels of the transmitted electric field strength greater or equal than 100 V/m. Seven of these (C0HC, C2EM, F0GF, M0GM, N0GM, N1IP and N3DF) frequently showed peaks at 6 GHz at 200 mm and 500 mm distance. F0GF, M0GM, N0GM and N1IP showed also, in some cases, significant spectral content around and below 1 MHz. Especially F0GF showed rather strong peaks, about 20 dB above noise level. At 200 mm distance the 6 GHz level was 48.8 ±0.5 dB below the peak level at 3 GHz. Some of the pulses F0GF also show a low frequency spectral content. It is interesting to note that N0GM at 200 mm show 6 GHz peaks 51.9±1.5 dB below the peak level at 3 GHz and not any low frequency content, while at 500 mm distance data show 6 GHz peaks 51.3±1.0 dB below the 3 GHz level and also in some cases a low frequency content. In neither of the cases the relative low frequency content were as strong as for test object 38 at 500 mm distance (pulse 1), see paragraph 4.7.2, it rather compares with the same object at the distance 200 mm. It can also be noticed that in most cases there were no strong distortions of the pulses in time domain.

In Appendix E we show time- and frequency domain plot of all 10 pulses registered for test object F0GF at 200 mm distance.

5 Conclusions and Future Work

- No major degradation of the 31 corroded test objects could be detected after irradiation at high field levels.

- Most of the tested objects showed rather small changes of the time domain shape of the transmitted pulse. Also, most of the objects showed no, or rather small peaks at 6 GHz. In all cases the peak levels at 6 GHz were very much lower than the

corresponding peak levels at 3 GHz. This indicates only a very limited effect due non-linear behaviour. However, many of the cases that show enhanced peaks at 6 GHz also indicate a significant spectral content below and around 1 MHz. A preliminary analysis, which is however uncertain due the low sensitivity of the D-dot probe at low frequencies, indicates that the energy content at low frequencies might in several cases be of the same order as that around 3 GHz. This should be further evaluated in the future.

6 Future Work

A further evaluation of the low frequency data, which indicates large energy contents at low frequencies, probably due to envelope detection, should be made. This will probably require a new measurement set-up using an electric field probe having a much larger sensitivity at low frequencies.

7 Acknowledgements

The authors acknowledge Lena Sjögren at the Swedish Corrosion Institute (SCI) and the other partners in the SCI studies for providing us with the corroded test objects. We also acknowledge valuable help from and discussions with Lars Pettersson at FOI, Lena Sjögren at SCI and Ulf Jordan at Chalmers University of Technology.

The work was financially supported by the Swedish Armed Forces.

9 References

[1]. O. Lundén, “Användarhandledning för mätuppställningen för studier av elektriskt överslag med 700 kW S-bands magnetron”, FOI-D-0110—SE, september 2003. Swedish Defence Research Agency FOI, Sensor Technology, P.O. Box 1165, SE-581 11 Linköpng, Sweden (In Swedish).

[2]. W. L. Stutzman and G. A. Thiele, Antenna Theory and Design”, John Wiley &Sons, New York, 1981.

[3]. M Bäckström, O Lundén, ”Transmission Cross Sections of Apertures Measured by Use of Nested Mode-Stirred Chambers”, FOA-R--96-00359-3.2--SE, December 1996. Swedish Defence Research Agency FOI, Sensor Technology, P.O. Box 1165, SE-581 11 Linköpng, Sweden.

[4]. M. Bäckström, O. Lundén, and P.-S. Kildal, “Reverberation Chambers for EMC Susceptibility and Emission Analyses”, *Review of Radio Science 1999-2002*, Chapter 18, Wiley-Interscience, John Wiley &Sons, Inc., New York, 2002.

[5]. M. Bäckström, T. Martin and J. Lorén, “Analytical Model for Bounding Estimates of Shielding Effectiveness of Complex Resonant Enclosures”, in Proceedings of *The 2003 International Symposium on Electromagnetic Compatibility (EMC)*, Istanbul, Turkey, May 11-15, 2003.

[6]. Martin T, Bäckström M and Lorén J., "Semi-Empirical Modeling of Apertures for Shielding Effectiveness Simulations", *IEEE Transactions on Electromagnetic Compatibility*, Vol. 45, No. 2, May 2003.

[7]. CISPR/A and SC 77B, IEC 61000-4-21 – *Electromagnetic Compatibility (EMC), Testing and Measurement Techniques: Reverberation Chamber Test Methods*, Committee draft for vote (CDV), 26 June 2002.

[8]. Sjögren L, "Ageing of shielding joints", KI Report No 2004:2E, Swedish Corrosion Institute, Kräftriket 23A, SE-104 05 Stockholm, Sweden.

[9]. Persson D and Kucera V, "The effect of corrosion and degradation on the shielding properties of joints in electronic enclosures. Near field emission measurements.", KI Report No 1999:4E, Swedish Corrosion Institute, Kräftriket 23A, SE-104 05 Stockholm, Sweden.

[10]. Paul C R, "Introduction to Electromagnetic Compatibility", John Wiley & Sons, Inc., New York, 1992.

[11]. Jordan U, Andersson D, Kim A, Lisak M, Bäckström M, Lundén O, "Microwave Breakdown in Slots", Dep. of Electromagnetics, Report No 6, ISSN 1403-2724, Chalmers University of Technology, SE-412 96 Göteborg, Sweden, 2004.

[12]. Andersson D, Jordan U, Kim A, Lisak M, Lundén O, Bäckström M, Ferrer I, "Microwave Breakdown in Slots", in Proceedings of RVK02, Stockholm, Sweden, 10-13 June 2002.

[13]. Bäckström M and Lundén O, "Lägesrapport: Betydelsen av olinjära fenomen för giltigheten av lågnivå kopplingsmätningar", FOI Memo 03-1354, 2 June 2003, Swedish Defence Research Agency FOI, Sensor Technology, P.O. Box 1165, SE-581 11 Linköpng, Sweden.

[14]. Martin T, Bäckström M and Lorén J, "Transmission Cross Section of Apertures Determined by Measurements and FDTD Simulations", *Proc. of EMC Zürich'97, Session 46H5*, February 18-20, 1997. Zürich, Switzerland, pp. 245.

[15]. Pettersson L, "An S-band Digital Beamforming Antenna: Design, Procedures and Performance", FOA-R—99-01162-408--SE, December 1999. Swedish Defence Research Agency FOI, Sensor Technology, P.O. Box 1165, SE-581 11 Linköpng, Sweden.

[16]. http://www.prodyntech.com

APPENDIX A.

Photos of joints subjected to accelerated ageing (from first SCI study).

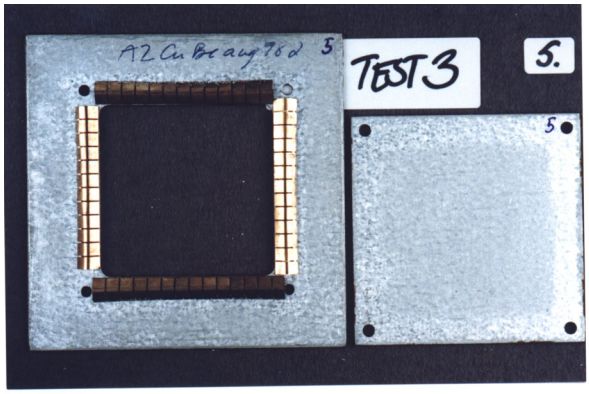

Figure A1. Object L5: Aluzink plate and lid, CuBe contact fingers after exposure to corrosion test 3 [9].

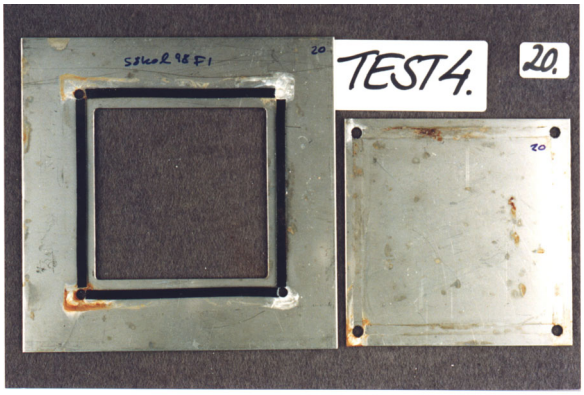

Figure A2. Object L20: Stainless steel plate and lid, carbon filled PTFE gasket, 3.2x1 mm (supplied by Gore). After exposure to corrosion test 4 [9].

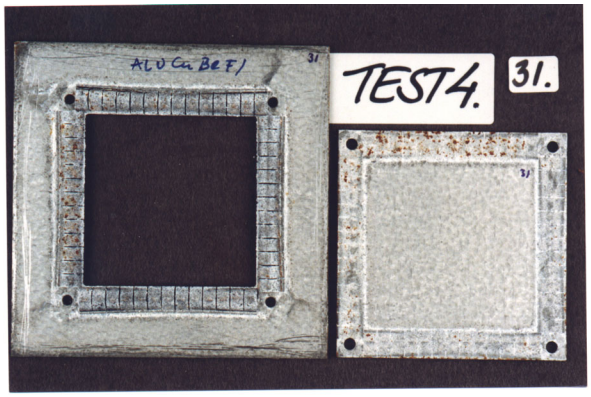

Figure A3. Object L31: As for L5, but corrosion test 4 [9].

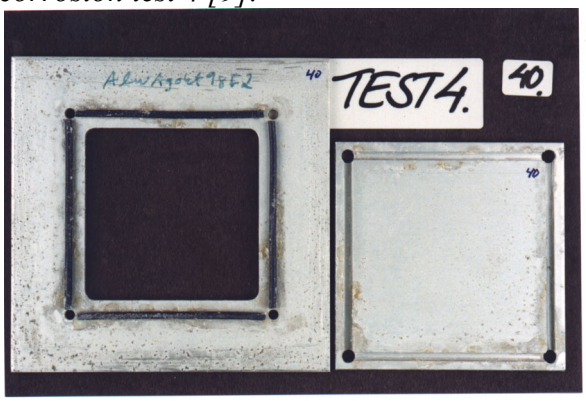

Figure A4. Object L40: Clear chromated aluminum plate and lid, silver filled elastomer. After exposure to corrosion test 4 [9].

APPENDIX B. Time-domain plots of magnetron pulses.

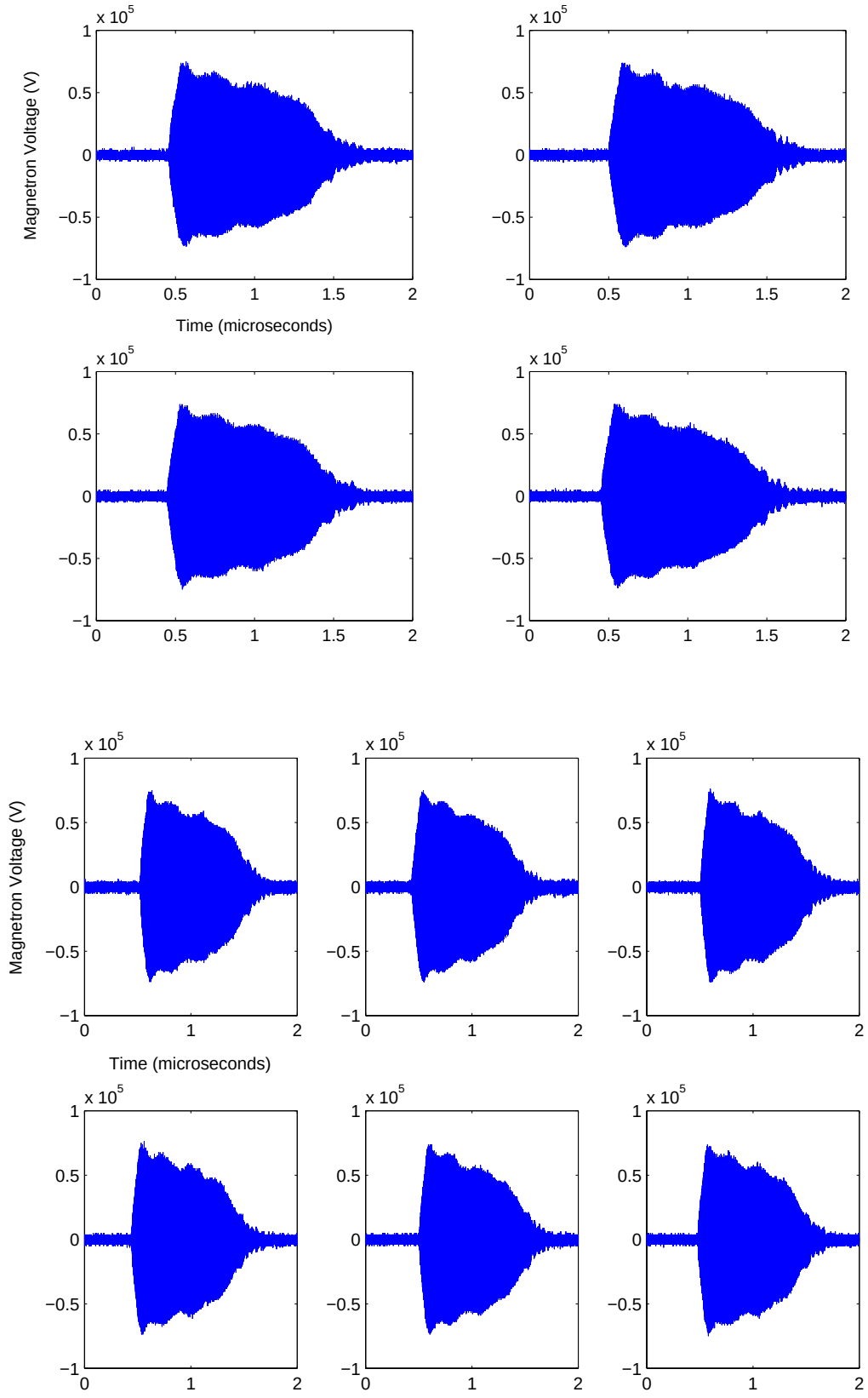

Figure B1. Pulses from magnetron measured in the reference port. Time-domain. File: UL_100_04011, pulses 1 to 10.

APPENDIX C. Frequency-domain plot for open hatch, solid hatch and slot.

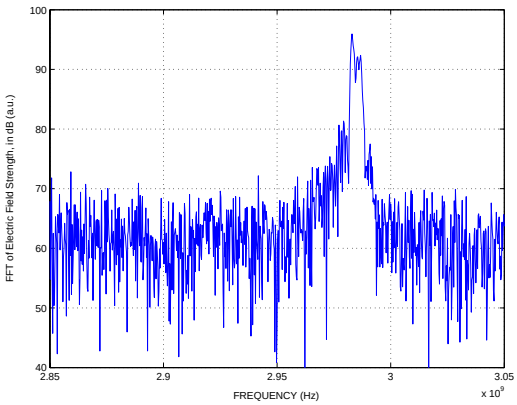

Figure C1. Pulse measured in test box with solid hatch. Frequency-domain, between 2.85 and 3.05 GHz. Solid_pytte_06_500_050225, first pulse.

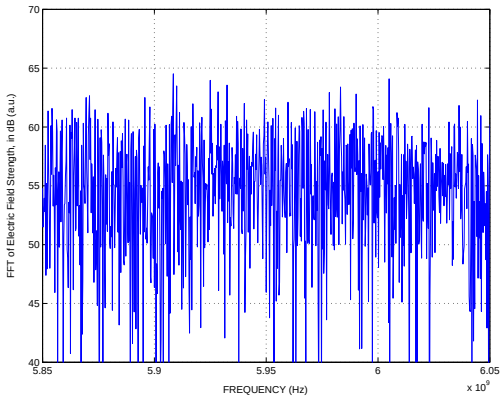

Figure C2. Pulse measured in test box with solid hatch. Frequency-domain, between 5.85 and 6.05 GHz. Solid_pytte_06_500_050225, first pulse.

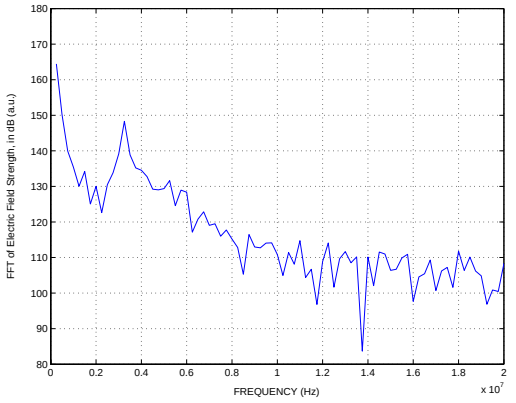

Figure C3. Pulse measured in test box with solid hatch. Frequency-domain, between 0 and 20 MHz. Solid_pytte_06_500_050225, first pulse.

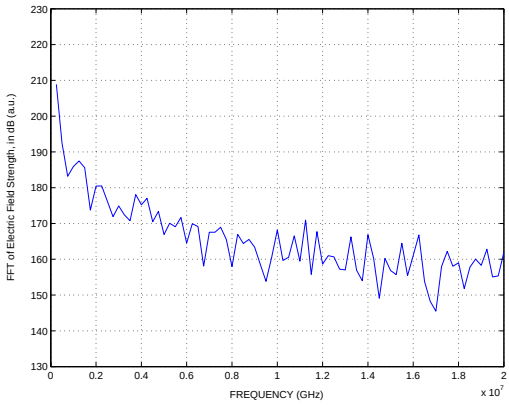

Figure C4. Pulse measured in test box with open hatch. Frequency-domain, between 0 and 20 MHz.
UL_100_040112, first pulse.

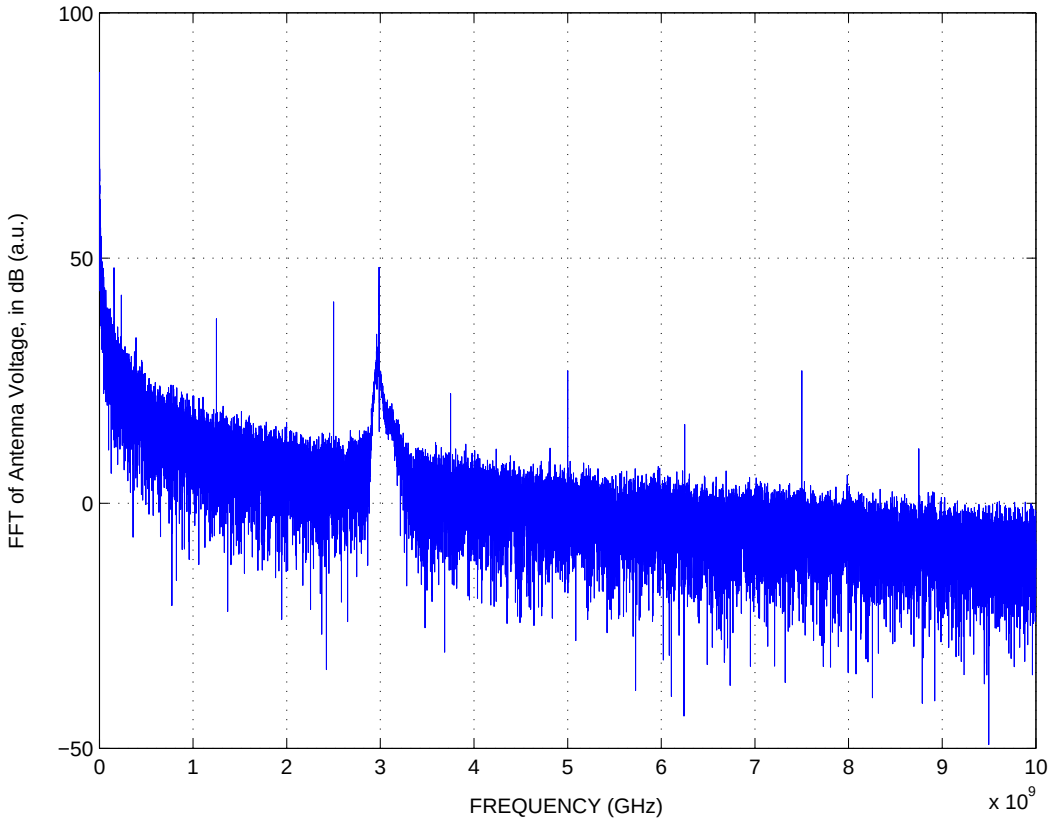

Figure C5. Pulse transmitted through the 46.3 x 0.1 mm slot. Distance 100 mm. $E = 52$ kV/m. Frequency domain, between 0 and 10 GHz.
S5_a100_1_030311.

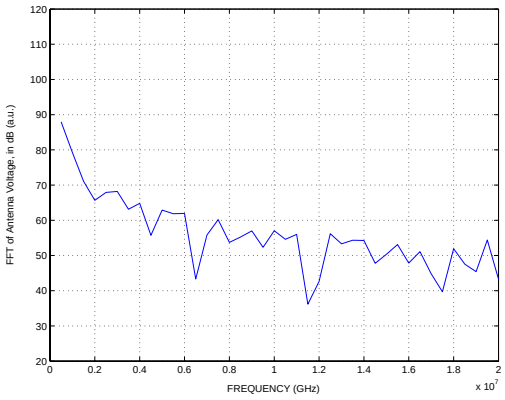

Figure C6. Pulse transmitted through the 46.3 x 0.1 mm slot. Distance 100 mm. $E = 52$ kV/m. Frequency domain, between 0 and 20 MHz.
S5_a100_1_030311.

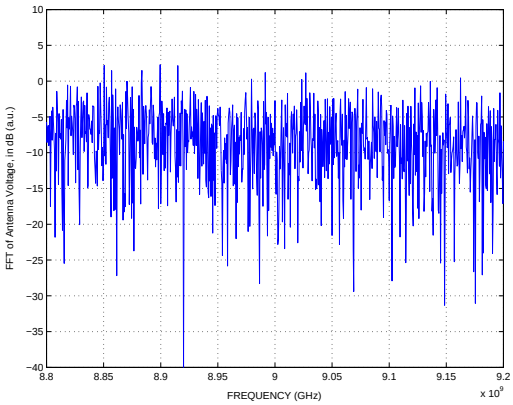

Figure C7. Pulse transmitted through the 46.3 x 0.1 mm slot. Distance 100 mm. $E = 52$ kV/m. Frequency domain, between 8.8 and 9.2 GHz.
S5_a100_1_030311.

APPENDIX D. Time- and frequency-domain plots for (mainly) test object L38.

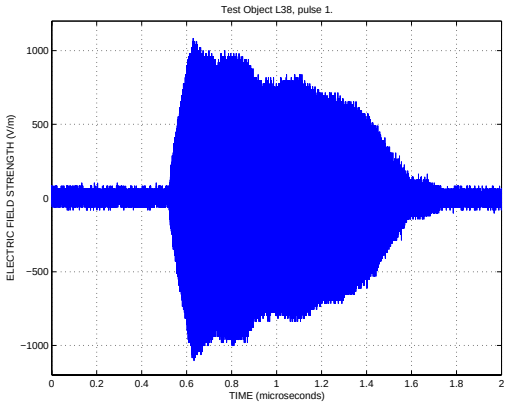

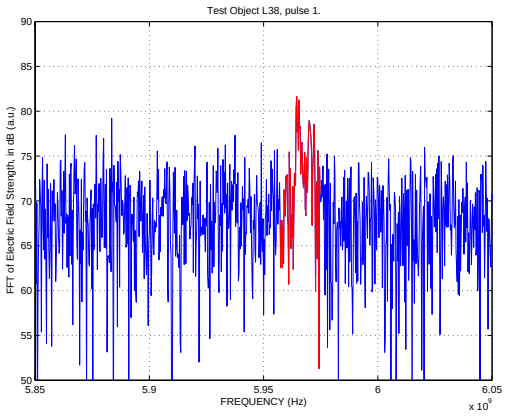

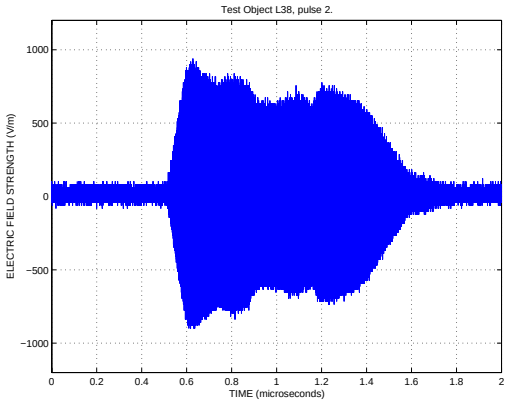

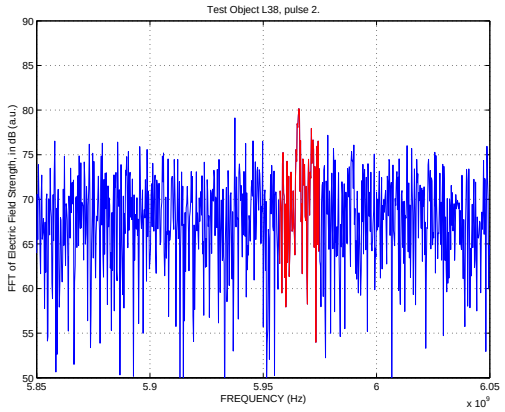

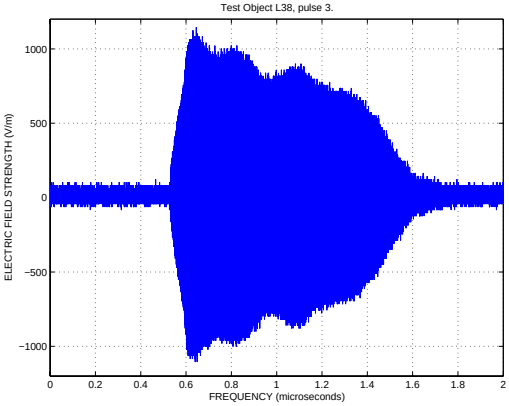

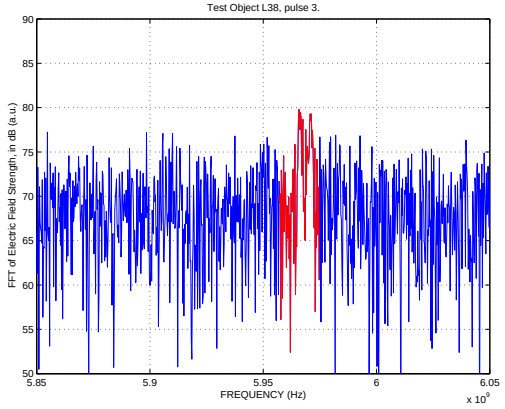

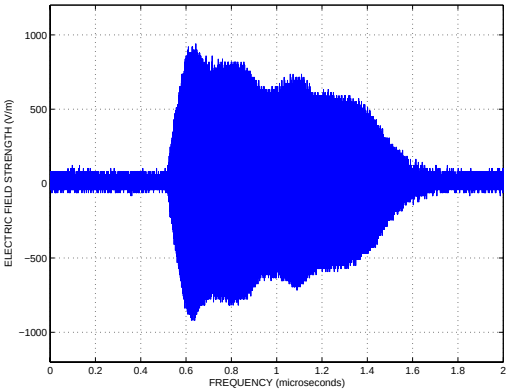
ELECTRIC FIELD STRENGTH (V/m)
FREQUENCY (microseconds)

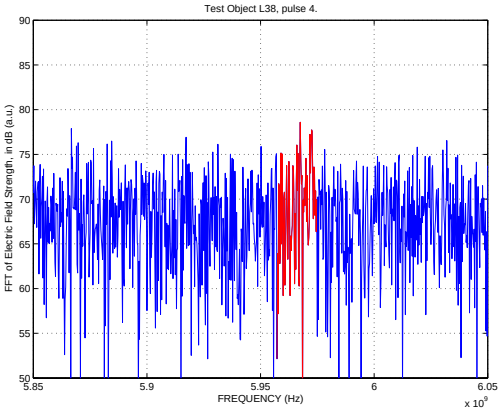
Test Object L38, pulse 4.
FFT of Electric Field Strength, in dB (a.u.)
FREQUENCY (Hz)
x 10^9

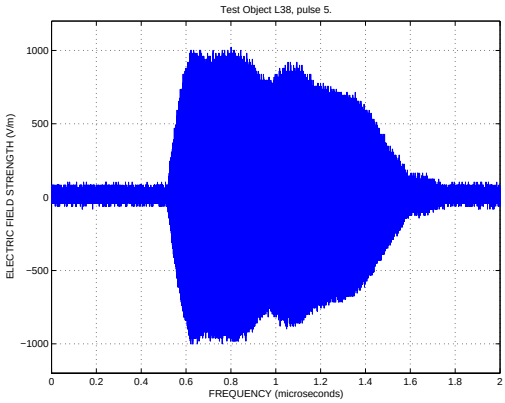
Test Object L38, pulse 5.
ELECTRIC FIELD STRENGTH (V/m)
FREQUENCY (microseconds)

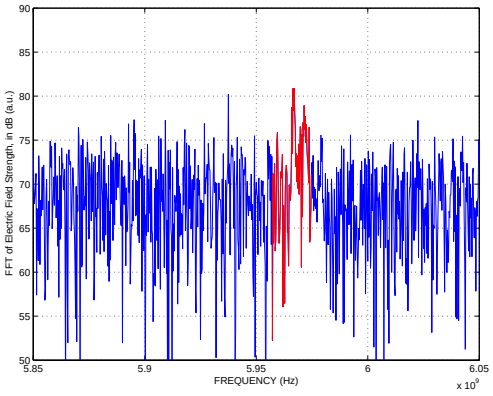
FFT of Electric Field Strength, in dB (a.u.)
FREQUENCY (Hz)
x 10^9

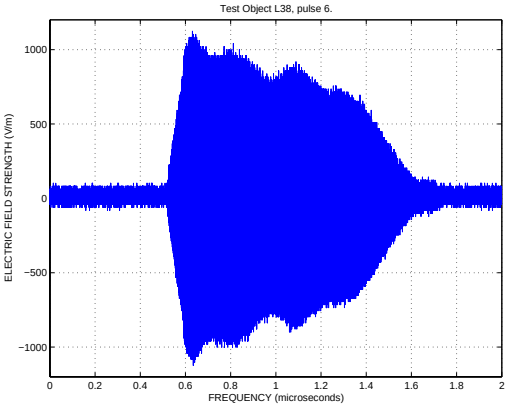
Test Object L38, pulse 6.
ELECTRIC FIELD STRENGTH (V/m)
FREQUENCY (microseconds)

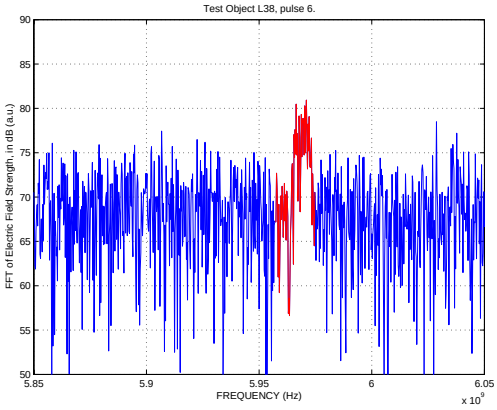
Test Object L38, pulse 6.
FFT of Electric Field Strength, in dB (a.u.)
FREQUENCY (Hz)
x 10^9

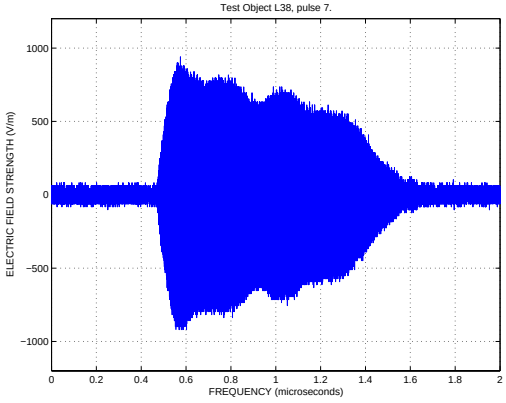
Test Object L38, pulse 7.
ELECTRIC FIELD STRENGTH (V/m)
FREQUENCY (microseconds)

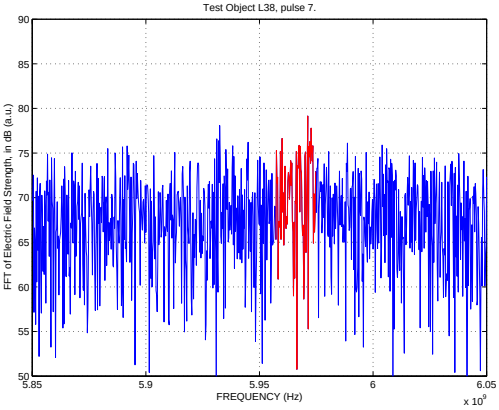
Test Object L38, pulse 7.
FFT of Electric Field Strength, in dB (a.u.)
FREQUENCY (Hz)
x 10^9

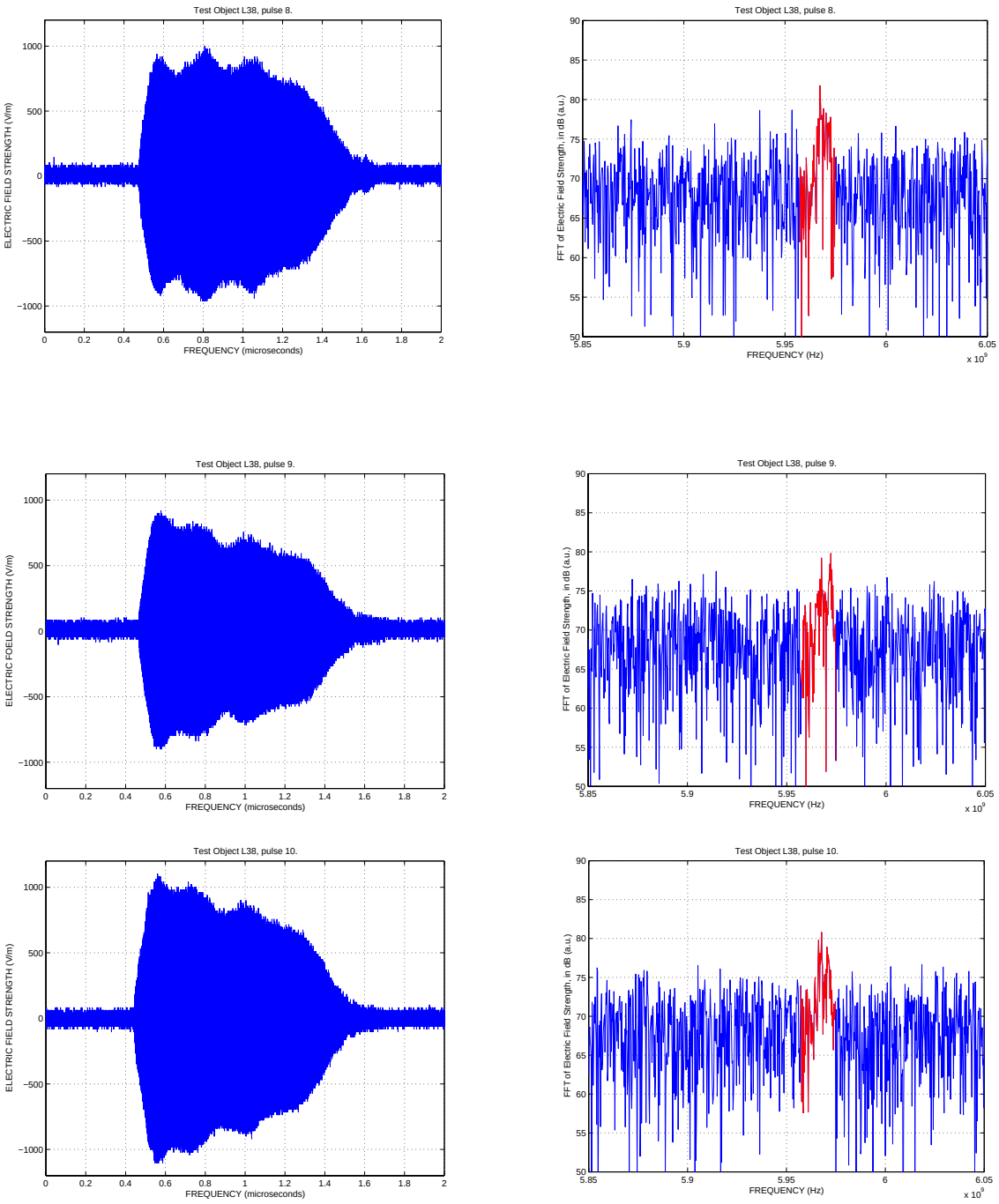

Figure D1. Time and frequency domain, between 5.85 and 6.05 GHz. Test object L38. Distance 200 mm. E = 38 kV/m.
L38_200_031218

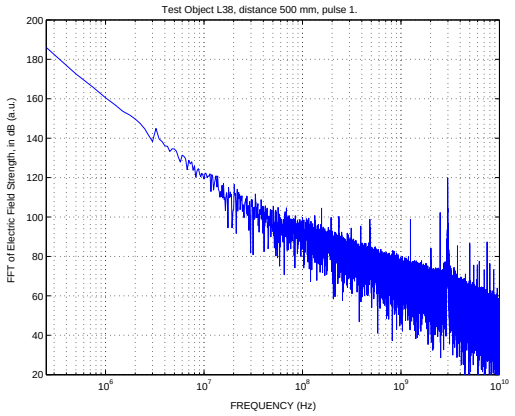

Figure D2. Pulse transmitted through test object L38. Distance 500 mm. Pulse 1. E = 21 kV/m. Frequency Domain, logarithmic frequency scale.
L38_500_031218.

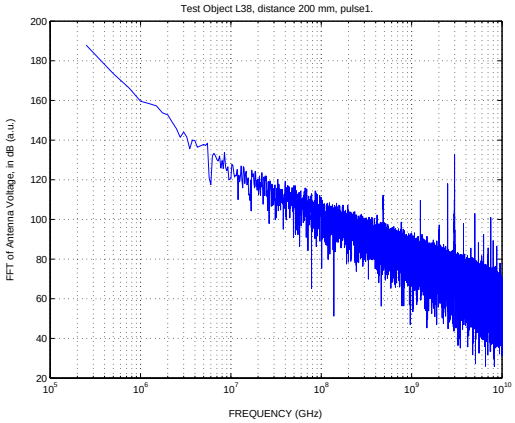

Figure D3. Pulse transmitted through test object L38. Distance 200 mm. Pulse 1. E = 38 kV/m. Frequency Domain, logarithmic frequency scale.
L38_200_031218.

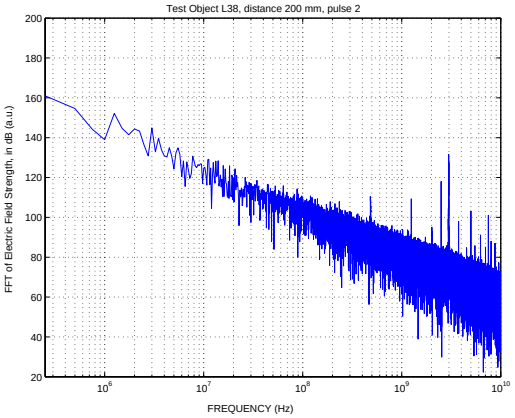

Figure D4. Pulse transmitted through test object L38. Distance 200 mm. Pulse 2. E = 38 kV/m. Frequency Domain, logarithmic frequency scale.
L38_200_031218.

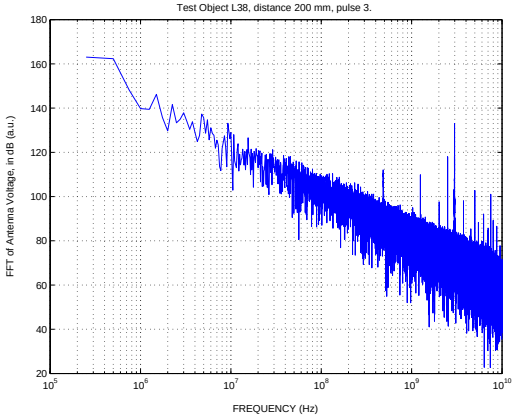

Figure D5. Pulse transmitted through test object L38. Distance 200 mm. Pulse 3. E = 38 kV/m. Frequency Domain, logarithmic frequency scale.
L38_200_031218.

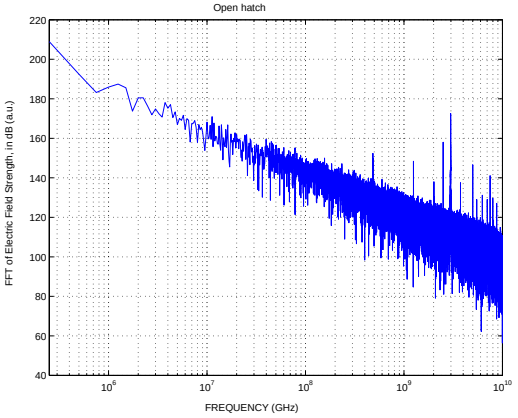

Figure D6. Pulse transmitted through open hatch. Distance 100 mm. Pulse 1. E = 53 kV/m. Frequency Domain, logarithmic frequency scale.
UL_100_040112.

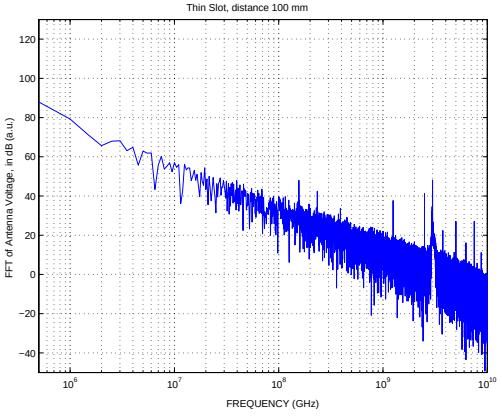

Figure D7. Pulse transmitted through the 46.3 x 0.1 mm slot, measured using a horn antenna. Distance 100 mm. E = 52 kV/m. Frequency Domain, logarithmic frequency scale. S5_a100_1_030311.

APPENDIX E. Time- and frequency-domain plot for test object F0GF.

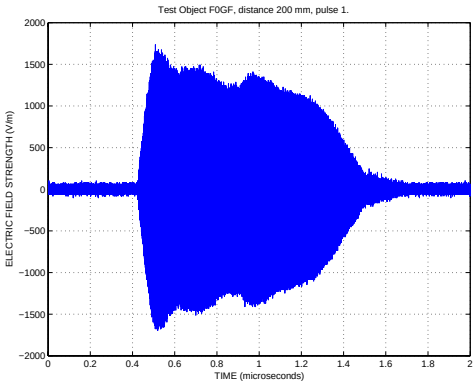

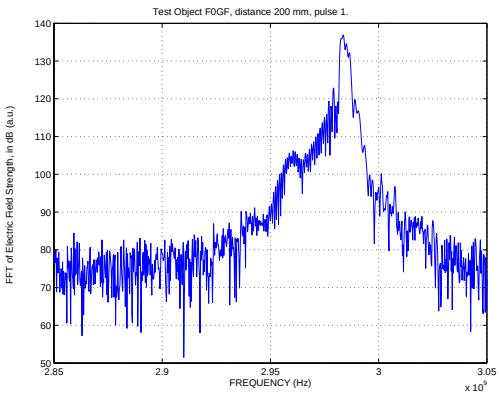

Pulse 1.

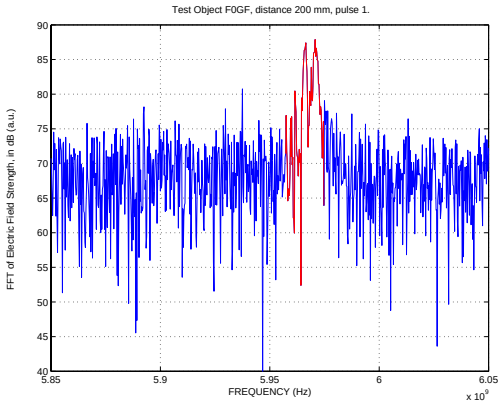

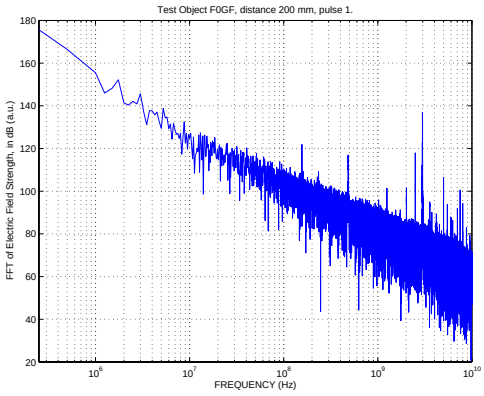

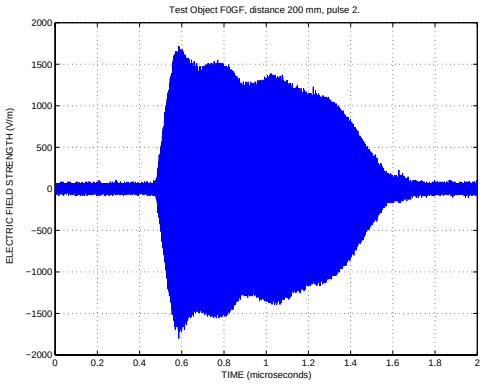

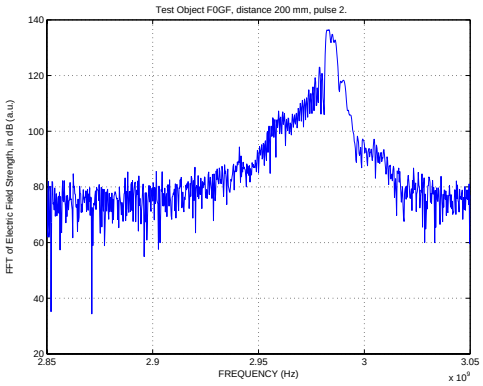

Pulse 2.

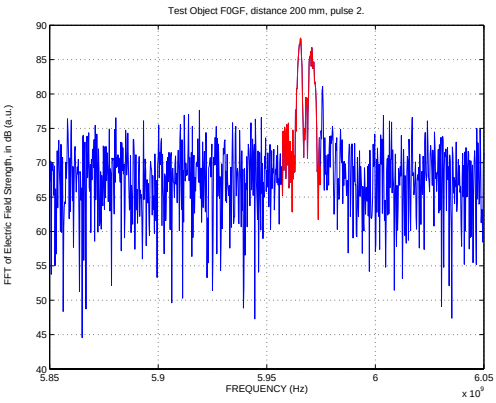

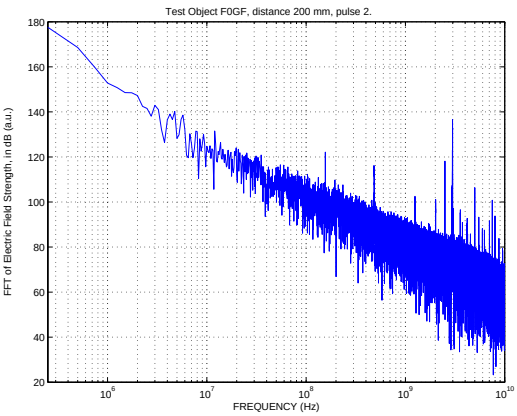

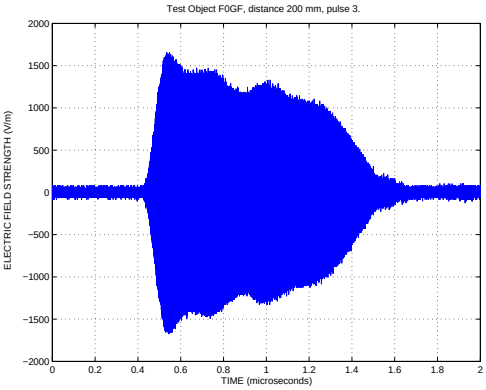

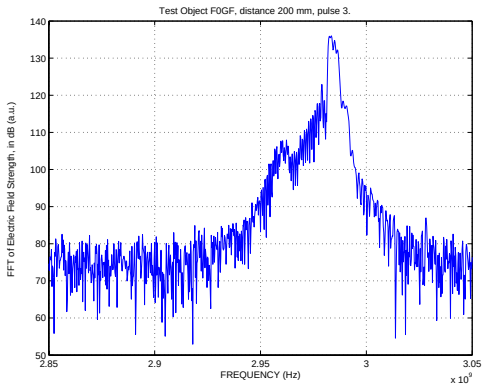

Pulse 3.

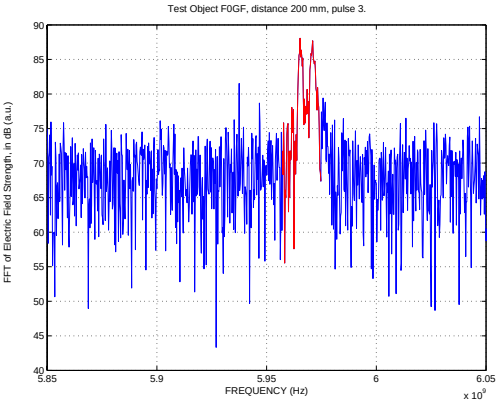

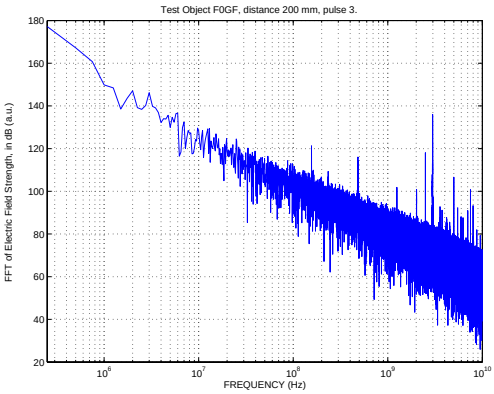

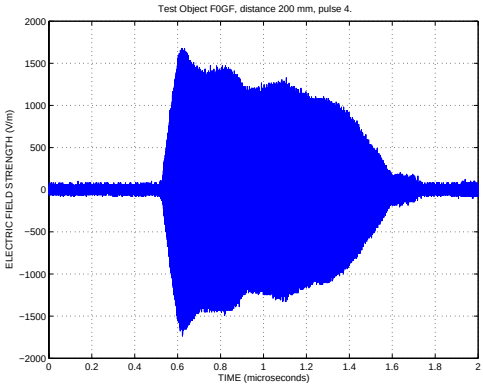

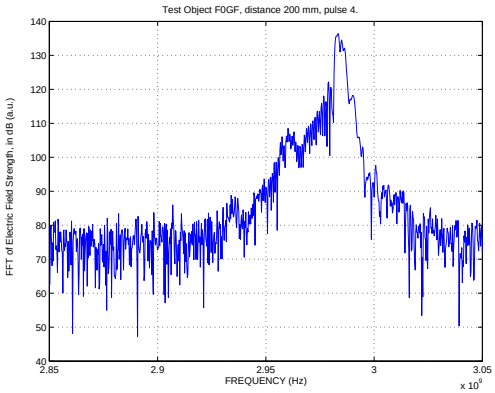

Pulse 4.

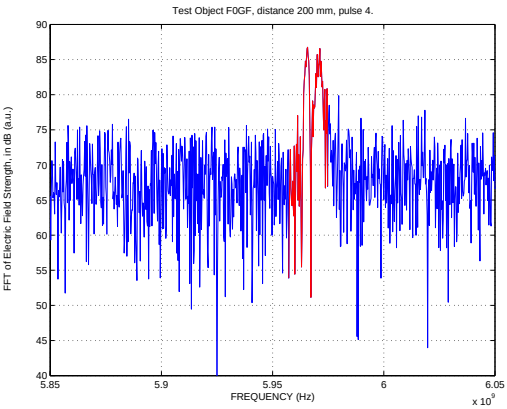

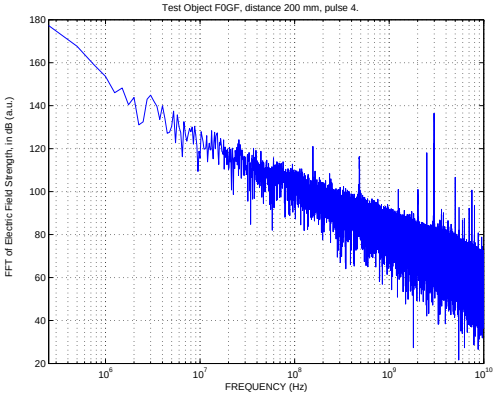

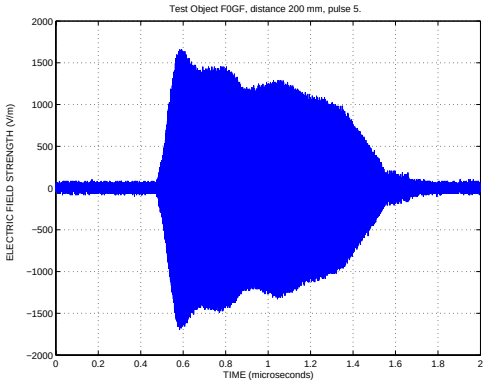

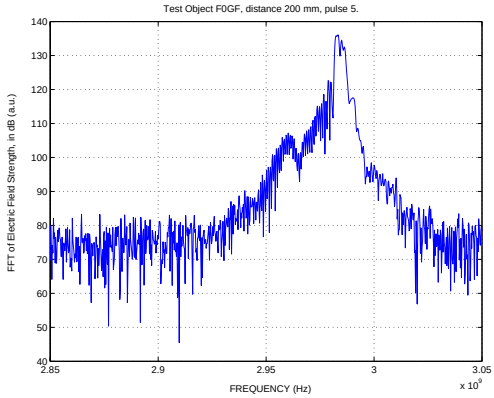

Pulse 5.

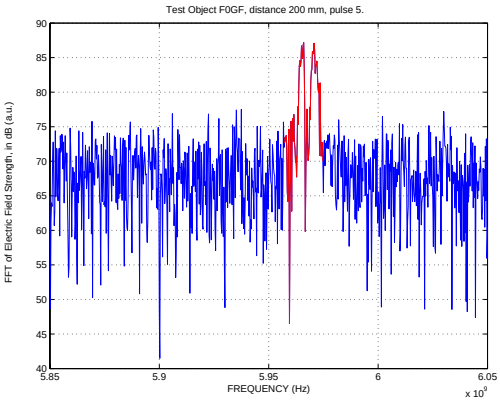

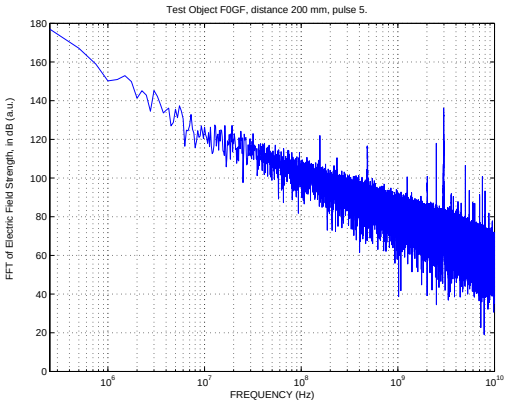

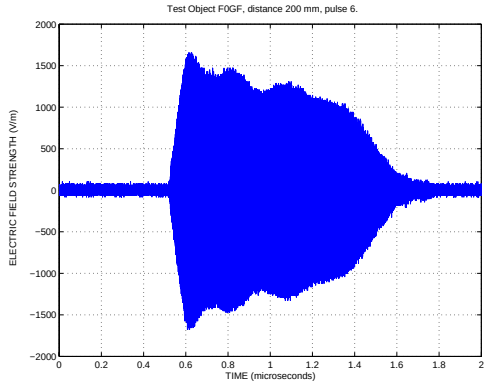

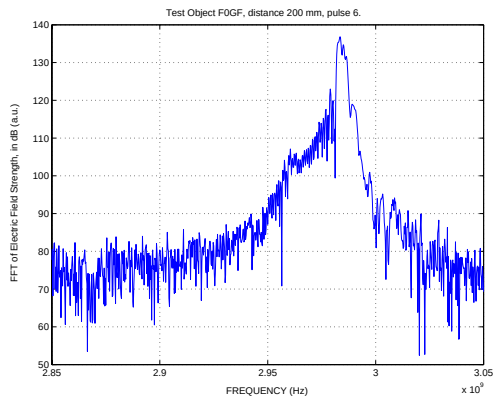

Pulse 6.

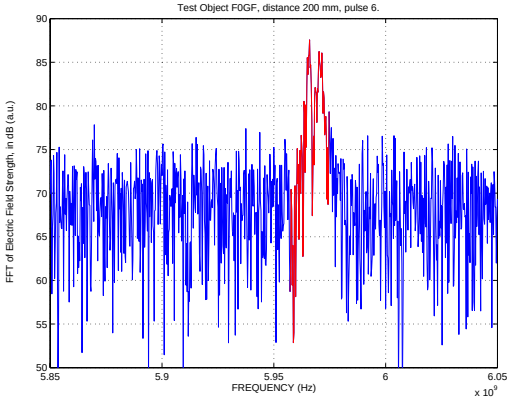

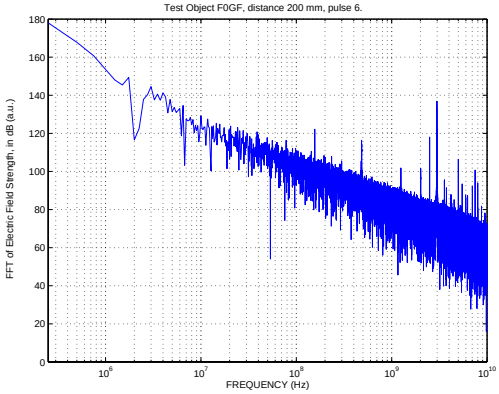

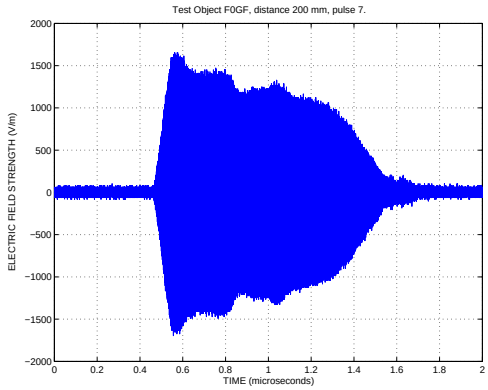

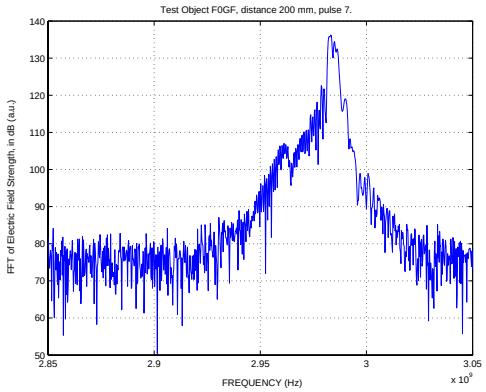

Pulse 7.

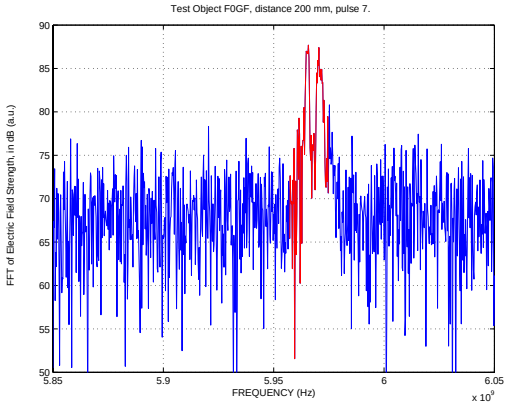

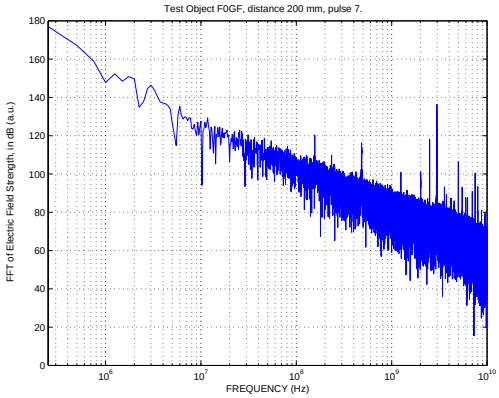

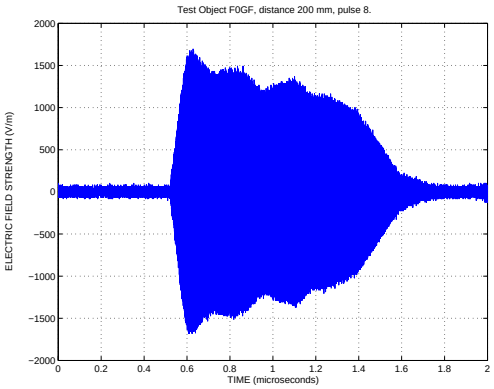

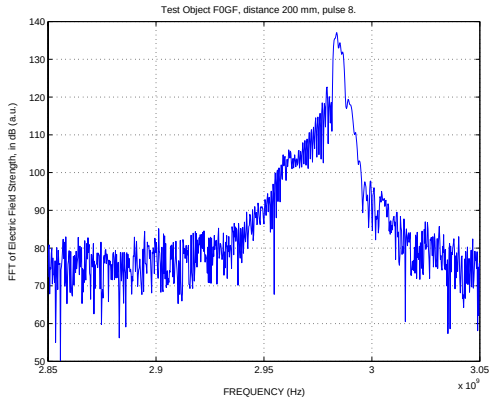

Pulse 8.

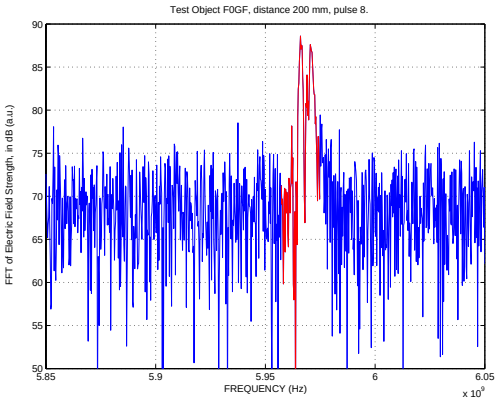

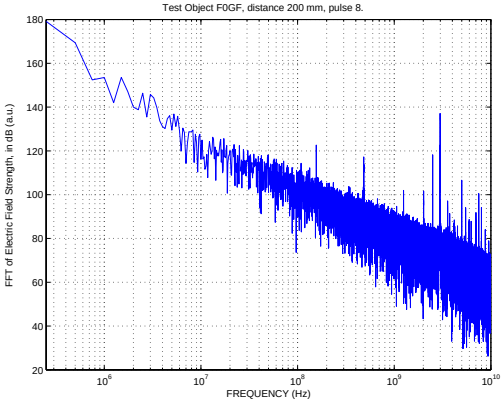

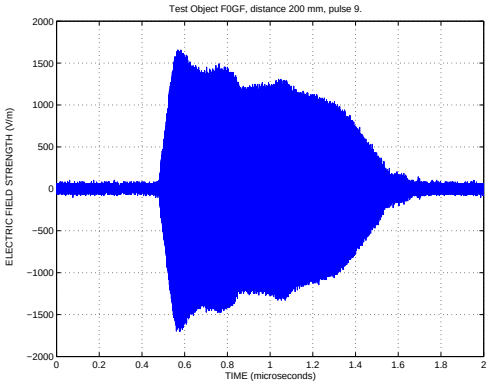
Test Object F0GF, distance 200 mm, pulse 9.
ELECTRIC FIELD STRENGTH (V/m)
TIME (microseconds)

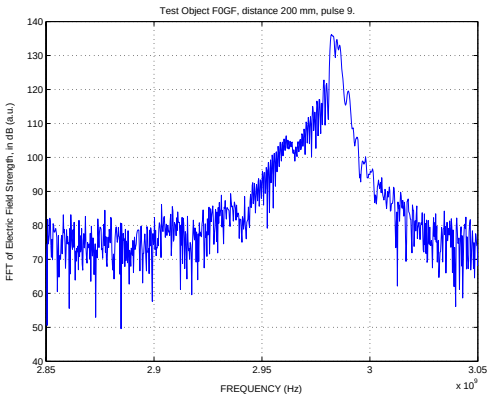
Test Object F0GF, distance 200 mm, pulse 9.
FFT of Electric Field Strength, in dB (a.u.)
FREQUENCY (Hz)

Pulse 9.

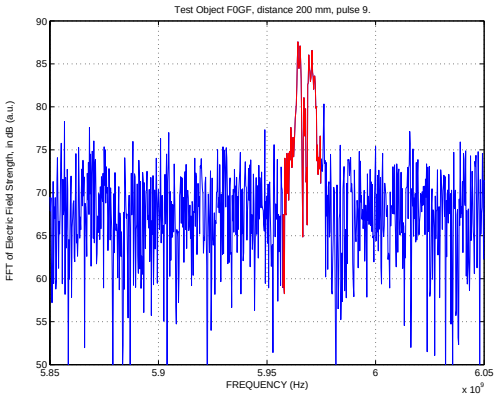
Test Object F0GF, distance 200 mm, pulse 9.
FFT of Electric Field Strength, in dB (a.u.)
FREQUENCY (Hz)

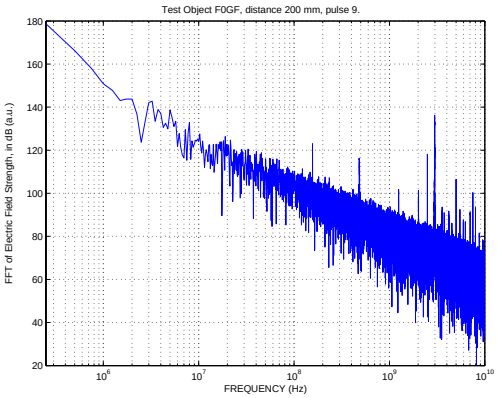
Test Object F0GF, distance 200 mm, pulse 9.
FFT of Electric Field Strength, in dB (a.u.)
FREQUENCY (Hz)

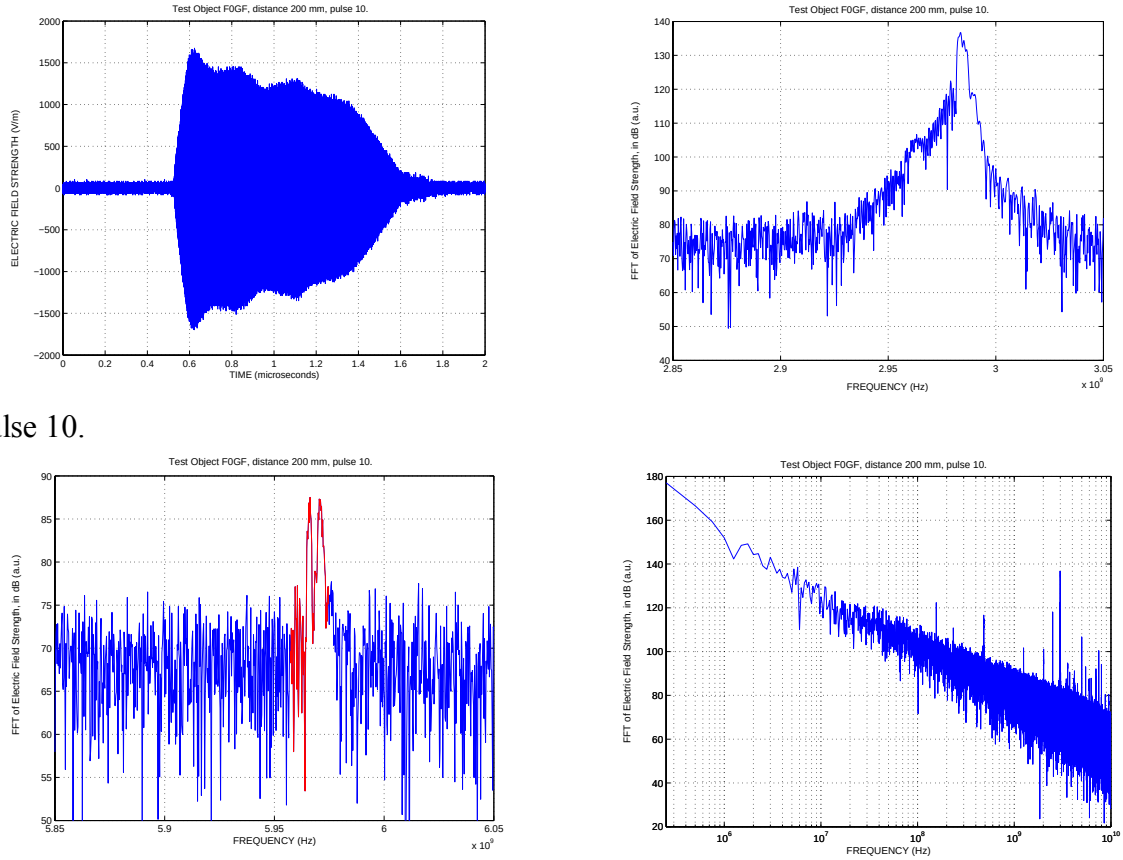

Pulse 10.

Figure E1. Time and frequency domain plots for test object F0GF, all 10 pulses. Distance 200 mm. E = 37 kV/m. For each pulse: Upper left: Time Domain; Upper right: Between 2.85 and 3.05 GHz; Lower left: Between 5.85 and 6.05 GHz; Lower right: The complete frequency interval using logarithmic frequency scale.
F0GF_200_040225